Horizontal tectonics assembled unrelated crustal blocks in the Paleoarchean

Mudlappa Jayananda (mjayan.geol@gmail.com)
University of Hyderabad https://orcid.org/0000-0002-2518-231X
Martin GUITREAU
Université Clermont Auvergne https://orcid.org/0000-0001-7156-6536
Aadhiseshan Krishnaswami Ravindran
University of Hyderabad
Sun-Lin Chung
National Taiwan University https://orcid.org/0000-0002-5362-4496
Takashi Miyazaki
Japan Agency for Marine-Earth Science & Technology (JAMSTEC) https://orcid.org/0000-0002-0889-3961

Article

Keywords: horizontal tectonics, crustal blocks, Paleoarchean

Posted Date: December 11th, 2020

DOI: https://doi.org/10.21203/rs.3.rs-122833/v1

Horizontal tectonics assembled unrelated crustal blocks in the Paleoarchean

M. Jayananda[1*]., Martin Guitreau[2], K.R. Aadhiseshan[1], S.L. Chung[3]., T. Miyazaki[4]

1. Centre for Earth, Ocean & Atmospheric Sciences, University of Hyderabad, Gachibowli, Hyderabad -500 046, India

2. Université Clermont Auvergne, IRD, CNRS, OPGC, Laboratoire Magmas et Volcans, UMR 6524, F-63000 Clermont-Ferrand, France

3. Institute of Earth Sciences, Academia Sinica, Nangang, Taipei 11529, Taiwan

4. Research Institute for Marine Geodynamics (IMG), Japan Agency for Marine-Earth Science & Technology (JAMSTEC), Yokosuka, Kanagawa 237-0061, Japan

** corresponding author*

Abstract

Archean geodynamics and craton formation are topics of much debate for decades. Here we present new evidence from field, petrography, geochronology, elements and Nd-Hf isotope geochemistry for origin of Paleoarchean micro-blocks in different geodynamic environments and their assembly into cratonic framework through horizontal motion. The cratonal core in the western Dharwar craton, southern India formed through assembly of three genetically unrelated micro-blocks: a microcontinent with oceanic plateau remnants, an oceanic arc, and a section of oceanic lithosphere. Isotopic age data from these micro-blocks and surrounding basement gneisses indicate that the assembly of micro-blocks marked by intrusions of hot trondhjemite magmas that drive partial convective crustal overturn, thus resulting in dome-and-keel structures visible in the Archean cratons. Our study reveals horizontal motion of unrelated tectonic units during the Paleoarchean, while mantle plumes driven vertical accretion contributed to major crustal growth allowing geodynamic linkage between Paleoarchean cratons.

Debate on Archean tectonics

Tectonics of the evolving early Earth, origin of protocontinents and craton formation are topics of much debate in Earth and Planetary Sciences. Present day dynamics of the planet Earth is driven by plate tectonics but when this regime initiated and what kind of processes were in operation during Archean has remained highly controversial for decades[1-2]. Several hypotheses have been put forth such as heat-pipe[3], stagnant lid[4], plate tectonics[5], mixed models[6], and some authors emphasize the evolution of processes and/or the transition between specific regimes[7-8]. Major arguments for Archean geodynamics are based on lithological assemblages[9-10], tectonic fabrics[11-12], geochemistry[13-14], geophysics[15], and numerical modeling[16-17]. Subduction is often argued as major process to explain geochemistry and origin of TTGs and mafic rocks (e.g.,[18-19; 2]) but non-uniformitarian models involving melting of stagnant lid by plumes have also been proposed[20-21]. A central aspect of this uncertainty relies on how one interprets Archean greenstone belts. Do they represent oceanic crust[3,10], oceanic plateaus[22], or back-arc basins[23] and what is their relationship with adjoining granitoids?

Archean cratons differ from their present-day counterparts by exhibiting strong dichotomous lithologies made of greenstone belts (ultramafic to mafic lavas, detrital and chemical sediments) and granitoids (TTG; tonalite-trondhjemite-granodiorite, e.g.,[24]). The geodynamic context of formation and processes responsible for their association are still disputed (e.g.,[4,21,25-26]). Addressing these issues is crucial as they bear a great deal on the thermal and chemical evolution of the early Earth, formation of habitable continents and emergence of biosphere. Here we address the geodynamic context of Archean crustal growth and craton formation from our target study in the Western Dharwar Craton (WDC), Southern India (**Fig.1**). We assess evidence for role of vertical accretion in building of early protocrust

as well as role of horizontal motion in assembly unrelated micro-blocks leading to craton formation. Addressing this question is key to unravel the geodynamics of Archean Earth and this is the purpose of the present contribution.

Western Dharwar craton (WDC) - An ideal target

The WDC is an ideal target to address Archean geodynamics because it forms a wide time (3600-3200 Ma) and tectonic window with typical dome-keel architecture from mid-to lower crustal levels due to northward tilting[27-29]. The cratonal core in the vicinity of Holenarsipur greenstone belt[30] preserves ca. 3430-3270 Ma granitoids of tonalite-trondhjemite-granodiorite (TTGs) - greenstone assemblages which in turn intruded by ca. 3200 diapiric trondhjemites[31-32] coinciding with development of regional dome and keel patterns[33]. Yet, older crust played a role in the formation of the WDC as evidenced by >3450 Ma detrital and inherited zircon crystals ([34,32,this study]) as well as by Hf, Nd and Pb isotope signatures[35,31-32]. However, mechanisms and tectonic context of crust accretion are debated as the greenstone sequences and adjoining granitoid basement have been interpreted as oceanic plateau and island arc[31,36-37] flat subduction of plume fed oceanic plateau crust[38], remnants of migrating oceanic crust from spreading centre to trench[39]. Holenarsipur greenstone belt is considered to be a collage of two distinct stratigraphic units[40], for which various types of data presented including geological[41] strain fabrics[33], elemental and isotope data ([31-32,37-38,42-43]). Here we present a multidisciplinary study on the Holenarsipur greenstone belt and adjoining TTGs that allows identification of distinct tectonic blocks and their assembly through horizontal motion which further discussed on global scale in the light of data from other cratons.

Three tectonic blocks

Field, elemental, Nd-Hf isotope data revealed three tectonic units that we labelled Southwestern, Northcentral, and Eastern blocks (**Fig.1**).

The Southwestern block comprises dominant metamorphosed ultramafic volcanic rocks with minor mafic rocks associated with sediments and adjoining TTGs. Abundance of ultramafic-mafic rocks gradually increases from large discontinuous outcrops within the granitoids to continuous outcrops from south to north of the southwestern block. The ultramafic rocks occasionally forming pillows with chilled margins indicating eruption in marine environment. The adjoining ca.3430-3300 Ma TTGs are intruded by ca. 3200 Ma diapiric trondhjemites.

The Northcentral block comprises dominant greenstone assemblages including ultramafic to mafic volcanics with minor felsic pyroclastic flows and interlayered pelites. The greenstone unit fragmented by the intrusion of ca. 3200 Ma diapiric trondhjemites (**see fig.1**). Ultramafic-mafic rocks erupted in marine environment as revealed by crude pillows and flow top pillow breccias. Felsic volcanics are confined to higher stratigraphic levels erupted in sub-aerial environment. Chlorite-chloritoid-garnet bearing pelitic sediments along southern boundary imply ultramafic to mafic provenance and deposited in oceanic environment far from sizable continent. These characteristics of the greenstone assemblages points to oceanic arc setting. The greenstone volcanics show the imprints of contact metamorphism along their contact zone with ca. 3200 Ma diapiric trondhjemite as evidenced by large randomly oriented actinolite, tremolite and hornblende crystals. Numerous quartz-veins with large tourmaline crystals inject into the greenstone volcanics along the contact zone with diapiric trondhjemite.

The Eastern block is a thin (500 m to 3 km width) elongated volcanic-sedimentary assemblage that runs for about 60 km in north-south direction (Line B of Fig.1). In its northern part, an E-W road cut displays a complete section of volcano-sedimentary sequence. From east to west, the sequence begins with pillowed mafic-ultramafic rocks with chilled margins followed by phyllite clays, chert layers, BIFs, several fine grained sheeted mafic dykes, plagiogranite, gabbros to layered gabbros, fine grained ultramafic rocks to medium grained

peridotitic komatiites to the westernmost part (**Fig. 2a, b**). Further west, peridotitic komatiites show tectonic contacts with surrounding TTGs. The southern part of it corresponds to deeper level that displays talc-tremolite, actinolite-hornblende schist, gabbro-anorthosite and plagiogranite and peridotitic komatiites along east - west section. These two E-W cross-sections could correspond to a titled panel of preserved oceanic crust close to a spreading centre (**Fig. 2c**).

The contact relationships between the three tectonic units are key in understanding crustal architecture and assembly of these distinct blocks into cratonal framework. Sedimentary assemblages found along the margins of each block imply distinct tectonic settings. Along the northern limit of Southwestern block a thick quartzite with crossbedding and ripple marks is followed by quartz-pebble conglomerate which mark shallow shelf conditions with a dominant granitic source. These quartzite-conglomerate layers are followed by quartz-mica-kyanite-staurolite-garnet bearing pelite associated with ultramafic rocks and TTGs that indicate mixed provenance forming a possible continental nucleus with oceanic plateau fragments. The chlorite-chloritoid-garnet bearing pelite of the Northcentral block found along its southern margin consistent with oceanic setting. Within the Eastern block, close to the contact with the Northcentral block, a polymict conglomerate without any clast supported framework[40] containing sparse angular fragments of greenstone volcanics/sediments with fine grained matrix indicate local fragmentation within the basin. An interpretative south-west to north-east cross-section covering three blocks (Line A of Fig. 1) display fundamental architecture of the cratonal core showcasing vertical motions driven by body forces followed by crustal shortening (**Fig. 3**).

Timing of greenstone volcanism and adjoining basement granitoids

In the southwestern block, the contacts between greenstone ultramafic rocks and TTGs are tectonized. It is difficult to provide precise ages for ultramafic volcanism as $^{147}Sm/^{144}Nd$ ratios of samples were affected to some extent by fluid flow associated with metamorphism and emplacement of ca. 3200 Ma diapiric trondhjemites. Ultramafic to mafic rocks of all the three blocks together define Sm-Nd whole rock isochron age of 3028 ±53.3 Ma (MSWD = 2.3, figure not given) which represents cooling path of amphibolite facies event dated at 3091±12 Ma[31]. The ultramafic-mafic volcanics of Southwestern block define Sm-Nd whole rock isochron age of 3029±91.5 Ma (MSWD 1.2, figure is not given) which coincides with metamorphic cooling. The occurrence of ultramafic-mafic volcanics as large disrupted fragments within ca. 3400-3350 Ma TTGs in Southwestern block imply that volcanics erupted prior to 3350 Ma.

U-Pb zircon ages of this study together with published zircon ages[31-32,43] of adjoining TTGs reveal three major stages of accretion. Zircon xenocrysts from trondhjemite to granite[32] and granodiorite of this study indicate first stage accretion ca.3610-3500 Ma (see Fig. 5a in supplementary file). Our U-Pb zircon data of tonalitic to granodioritic gneisses reveal second episode ca. 3468-3410 Ma (supplementary file Fig. 5b-c) whilst zircon ages of several tonalitic to granodioritic samples indicate ca. 3350-3300 Ma (see fig. 5d-j in supplementary file) corresponding to third stage of TTG accretion.

The ultramafic-mafic volcanics of Northcentral block define an imprecise Sm-Nd isochron age of 3124±249 Ma (MSWD 2.1) which probably corresponds to metamorphic cooling. However, our U-Pb zircon data from pyroclastic felsic flow from highest stratigraphic levels define 3305±10 Ma (see fig. 6c in supplementary file). TTGs adjoining to the Northcentral block yield zircon U-Pb ages of 3429±9 Ma and 3429±11 Ma (see fig. 6a, b in supplementary file) without any inherited cores. Stratigraphic relationships between greenstone

153 and adjoining TTGs remain uncertain due to tectonized contacts but 3305±10 Ma pyroclastic
154 flows may represent a terminal stage of greenstone volcanism.
155 The greenstone volcanics of the Eastern block provide Sm-Nd whole rock isochron age
156 of 3345 ± 111 Ma (MSWD=1.8;figure is not given) which is close to U-Pb zircon of 3347±11
157 Ma of plagiogranite (fig.7 in supplementary file) interlayered with gabbroic rocks in the
158 northern roadcut which probably marks terminal stage of volcanism. Published U-Pb zircon
159 ages of basement TTGs from the western margin of the Eastern block indicate younger ages of
160 3276±5 Ma[31] and 3289 ±5 Ma[43].
161
162 *Geochemical fingerprinting of three tectonic blocks*
163 The petrogenetic interpretations were made on samples devoid of evident alteration and
164 weathering. However, exact petrological type of ultramafic-mafic rocks from three blocks may
165 not be good indicators of their origin, but geochemical signatures can help constrain source
166 reservoirs and unravel the geodynamic context of formation of such rocks (e.g.,[18,44]).
167 Major elements of volcanics from three greenstone units plotted on triangular diagrams
168 (Al_2O_3-Fe_2O_3+TiO_2- MgO **Fig. 4a**;[73]) and (CaO-MgO-Al_2O_3 **Fig.4b**,[74]) reveal dominant
169 komatiite to komatiite basalt composition whilst exhibit distinct trace element signatures
170 marking independent histories.
171 *Southwestern block – Oceanic plateau with remnants of microcontinent*
172 Incompatible elements content (REE, Nb, Y, Th, Zr; Fig. 8a-d and data table in
173 supplementary file) reveal two groups. The low REE group (ΣREE = 4.77-19.17 ppm with
174 lower SiO_2 44.09-45.97 wt%) exhibit flat to slightly fractionated REE patterns (Fig. 8a in
175 supplementary file) with $(Gd/Yb)_N$ 0.53-1.86 indicating their derivation by high degree melting
176 of shallow depleted mantle without significant residual garnet. This is consistent with absence
177 of Nb anomalies together with positive Zr and Y anomalies on primitive mantle[71] normalized

178 spider diagram (Fig.8b in supplementary file). The high REE group (ΣREE = 20.6-66.6 ppm)
179 with fractionated REE [$(Gd/Yb)_N$ 1.22-2.29, Fig.8c in supplementary file] together with
180 positive Nb, coupled negative Zr and Hf anomalies on spider diagrams (Fig.8d in
181 supplementary file) suggest origin of melts from deeper primitive mantle with possible residual
182 majorite?.

183 Initial $^{143}Nd/^{144}Nd$ ratios of komatiites were used to calculate $\varepsilon Nd_{(T=3400\ Ma)}$ values to
184 constrain mantle sources and possible crustal contamination. Nine samples with large range of
185 values ($\varepsilon Nd_{(T)}$ =0.4 to 3.7) suggest chondritic to depleted mantle reservoirs whilst two samples
186 with negative ($\varepsilon Nd_{(T)}$ = -3.0 to -0.7) values (**Fig.5**) related to possible contamination of pre-
187 existing crust[32,35]. Plots of incompatible element ratios like Th/Yb versus Nb/Yb (**Fig. 6a**.
188 after[72]) and Nb/Y versus Zr/Y (**Fig.6b** after[44]) suggest primitive to depleted mantle whilst
189 Zr/Nb versus Nb/Th plot[44] attribute their eruption as oceanic plateaus (**Fig.6c**).

190 *Nortcentral block – Oceanic arc with coeval mini volcanic plateau fragments?*

191 Major element data (SiO_2 = 45.11 to 68.65 wt%; MgO = 23.92 to 1.29 wt%) reveal
192 komatiite, komatiite basalt, basalt to dacite in composition. Komatiites contain low to moderate
193 ΣREE (14.6-59.1 ppm), display flat REE patterns with $(Gd/Yb)_N$ ratios of 0.99-1.68 (Fig.9a in
194 supplementary file) whilst komatiite basalts show moderate to high ΣREE (27.3-138.0 ppm)
195 displaying flat to fractionated REE patterns [$(Gd/Yb)_N$ = 0.94-1.93)] (Fig. 9b in supplementary
196 file) implying heterogeneous mantle reservoirs whilst negative Nb anomalies coupled with
197 either positive or no significant Zr, Hf and Y anomalies on spider diagrams (Fig.9c,d in
198 supplementary file) suggest origin from shallower mantle. These elemental characteristics,
199 lithological association of komatiite-komatiite basalt- basalt- dacite points to oceanic arc
200 signatures. Incompatible element ratios like Th/Yb versus Nb/Yb (**see fig. 6a**) and Nb/Y versus
201 Zr/Y (**see fig. 6b**) indicate heterogenous reservoirs involving primitive to depleted mantle with

a half number of samples show modern N-MORB signatures whilst on Zr/Nb versus Nb/Th studied samples extending arc to oceanic plateau setting wherein komatiite may represent volcanic plateau fragment adjacent to oceanic arc (**see fig. 6c**). Initial Nd isotope ratios of ten samples ($\varepsilon Nd_{(T)}$=3300 Ma) showing 1.4 to 5.8 (three samples with $\varepsilon Nd_{(T)}$ = -5.6 to -0.9) suggest chondritic to depleted mantle source with traces of ancient crustal contamination (**see fig. 5**).

Eastern block – Oceanic spreading centre

The komatiitic to basaltic volcanics with SiO_2 ranging 42.74-50.03 wt% form two groups: low ΣREE and high ΣREE. Initial Nd isotope ratios of twelve samples (εNd(T)=3350 Ma) showing -0.8 to 5.5 (except for three samples with anomalous values $\varepsilon Nd_{(T)}$ = -18.3, -5.1 and -2.3). The low ΣREE (5.80-22.20 ppm) group displays flat patterns with depletion in LREE, poorly fractionated [$(Gd/Yb)_N$ = 0.61-1.38; Fig.10a in supplementary file] which suggests depleted mantle similar to N-MORB. Absence of Nb anomalies coupled with positive Zr, Y anomalies on spider diagram points to melts origin from shallow depleted mantle which is consistent with $\varepsilon Nd_{(T=3350\ Ma)}$ ranging from 2.5 to 5.5 (Fig. 10b in supplementary file). On the contrary, the high ΣREE (48.39-294.79 ppm) group shows fractionated REE (Fig.10c in supplementary file) patterns [$(Gd/Yb)_N$ = 1.16-1.96] coupled with positive Nb anomalies and negative Hf-Y anomalies on spider diagrams (Fig. 10d in supplementary file) which coupled with $\varepsilon Nd_{(T=3350\ Ma)}$ values (1.4 to -0.8) suggest deeper primitive mantle. Element ratios like Th/Yb versus Nb/Yb and Nb/Y versus Zr/Y indicate their origin from N-MORB to E-MORB sources (**see figs.6a, b**). Further, on Zr/Nb versus Nb/Th plot suggests shallow depleted to deep primitive mantle with affinities to modern N-MORB to E-MORB implying oceanic spreading setting (**see fig. 6c**).

Origin of adjoining TTGs

Different source rocks including the melting of oceanic crust in subduction zone[45-46], oceanic arc crust[47], subducting oceanic plateau[48] and stagnant lid/oceanic plateau in mantle upwelling zone[4] proposed for origin of Archean TTGs. The lower K_2O/Na_2O even at high SiO_2 levels (>75 wt%), HREE depletion and quartz-normative nature[49-51] of TTGs preclude their origin by direct melting of mantle peridotite rather suggest mafic source.

Southwestern block (3430-3300 Ma TTGs)

Elemental and isotope characteristics of TTGs reveal two major groups: Older (3468-3400 Ma) dominantly low- Al_2O_3 (<14 wt%) with trondhjemite to granite composition whilst few samples with high- Al_2O_3 (>14 wt%). The younger (3350-3300 Ma) gneisses with low Al_2O_3 (<13.5 wt%) to high-Al_2O_3 (>15%) show tonalite to granodiorite composition. The older gneisses show higher MgO (up to 1.73 wt%), Fe_2O_3 (upto 3.12 wt%) despite high SiO_2 (74-76%) together with variable total REE (36-336 ppm) and poorly fractionated REE (Fig. 13a in supplementary file) patterns [$(La/Yb)_N$=0.35-2.3], less pronounced negative Nb-Ta with positive Y anomalies (Fig. 13b in supplementary file) on spider diagrams argue for low-pressure melting of basaltic source without residual garnet. This is consistent with their sub-chondritic Nb/Ta ratios together with low Zr/Sm, Sr/Y, Gd/Yb and low $K_2O/(Na_2O+CaO$; **Fig. 7a,b,c**) suggesting low-pressure (≤10 kbar) melting. The two high- Al_2O_3 (>14 wt%) samples with higher Ba, Sr, REE (232-282 ppm and moderately fractionated REE (see fig. 13a in supplementary file) patterns [(La/Yb)=12.6- 27.6] with negative Nb-Ta-Ti anomalies (see fig.13b in supplementary file) originated by moderate pressure (12-14 kbar) melting of basaltic source with hornblende, plagioclase and traces of garnet in residue.

Melting of mafic source like modern-MORB with strong depletion in incompatible elements [(0.16 wt% K_2O, <2.88 ppm Rb and <29.2 ppm of Ba, $(La/Yb)_N$ =<0.84; Sr/Y= < 3.5,[52])] cannot produce melts of TTG composition. Experimental work[53], phase equilibrium

249 modelling[54] together with high content of incompatible elements and Nd-Hf isotope data
250 preclude sources similar to MORB or komatiite but invoke chondritic to enriched mafic
251 source[55-56]. Majority of petrologic and geochemical data together numerical models argue
252 against horizontal motion of plates prior to 3300 Ma (e.g[4,57-58]). Therefore, melting of
253 subducting oceanic crust can be ruled out for origin of >3400 Ma TTGs. Alternatively, melting
254 of thick undepleted basaltic[56] stagnant lid forming the base of oceanic plateau may be
255 considered. Low pressure (10-12 kbar) melting under high thermal gradient (>700ºC/Gpa,[56]),
256 in the mantle upwelling zone[4] can generate TTGs melts with low Sr/Y, Zr/Sm and Gd/Yb
257 ratios.

258 Our in-situ Hf isotope data of zircons together with published[32] data [$\varepsilon Hf_{(T)}$ = - 2.4 to
259 +2.3] of 3468-3400 Ma indicate short crustal history of their precursors and involvement of
260 ancient (>3600 Ma) crust (**Fig. 8**). This agrees with whole rock Nd isotope data ($\varepsilon Nd_{(T)}$ = 0.8
261 to -2.8) of oldest gneisses[31] and radiogenic Pb in feldspars of ca. 3400 Ma gneisses indicating
262 involvement of crustal protoliths as old as ca. 3800 Ma[35].

263 Among 3350-3300 Ma gneisses, the low- Al_2O_3 gneisses with higher SiO_2 (72-79 wt%),
264 high total REE (299-1211ppm), moderately fractionated REE patterns, (Fig.13c in
265 supplementary file) but less pronounced negative Nb-Ta-Ti but strong negative Sr anomalies
266 (Fig.13d in supplementary file) on spider diagrams coupled with low Sr/Y, Nb/Ta, Zr/Sm,
267 Zr/Nb, K_2O/(Na_2O+CaO ratios (**see figs 7a, b, c**) suggest low-pressure (10-12 kbar) melting of
268 chondritic to enriched basaltic source with residual hornblende and plagioclase. On contrary
269 the high- Al_2O_3 gneisses show lower SiO_2 (61-72 wt%) with high Ba-Sr, low total REE (68-
270 153 ppm), weak to strongly fractionated REE patterns [$(La/Yb)_N$=2.4-33.7)] without Eu
271 anomalies (see Fig. 13c in supplementary file) coupled with strong negative Nb-Ta-Ti but
272 positive Sr anomalies spider diagrams (see fig.13d in supplementary file). This coupled with
273 higher Sr/Y, Nb/Ta, Zr/Sm, Sr/Y, K_2O/(Na_2O+CaO (**see figs.7 a, b, c**) indicate moderate

pressure melting (12-15 Kbar) of mafic source with hornblende, garnet-ilmenite (±) in residue. Experimental constraints refined melting conditions for origin of TTGs[53] also indicate 12-15 kbar for garnet to stabilize in the residue.

In-situ Hf isotope [$\varepsilon Hf_{(T)}$ 2.1 to 3.7] of 3350-3300 Ma gneisses (**see fig. 8**) indicate their origin from short lived mafic crust with minor ancient crustal input which is in confirmity with published Nd isotope [$\varepsilon Nd_{(T)}$ = -0.6 to 2.1;[31]].

Melting of subducting oceanic crust originated at spreading centre can be ruled out as such source is depleted and cannot explain high content of incompatible elements of the TTGs[31,47-48,59]. On the other hand, their origin could be attributed to either melting of the oceanic plateau crust or oceanic arc crust in the realm of horizontal motion of stagnant lid crust. Melting of oceanic plateau crust (similar to associated >3350 Ma komatiites or komatiite basalts) generate melts depleted in incompatible elements and require large scale differentiation to explain high incompatible element contents of TTGs. Further, no evidence for melting of associated komatiites preserved despite they form keels and interlayered with high-pressure assemblages (garnet-kyanite). Alternatively, enriched mafic rocks of oceanic arc crust generated by shallow subduction of rocks making up a stagnant lid beneath volcanic plateau or built on substrate of ancient (>3600 Ma) crust can be considered. Moderate (12-15 kbar) melting of enriched mafic arc crust can generate TTGs melts with stable hornblende-plagioclase ± garnet ± ilmenite in residue. The 3350-3300 Ma gneisses appears to be sub-contemporaneous with volcanism in the Northcentral block as revealed by 3305±10 Ma pyroclastic felsic lava flows from the higher stratigraphic level. This sub-contemporaneous nature together with petrological data like increasing pressures from lower pressure in north (chlorite-chloritoid-garnet) higher pressure to the south (kyanite-garnet in contact) along the contact zone between Northcentral to Southwestern block imply southward convergence

298 probably built oceanic arc. Melting of newly formed oceanic arc crust at different depths could
299 generate the 3350-3300 Ma gneisses.

300 *Northcentral block: ca.3430 Ma TTGs*

301 TTGs adjoining to the greenstone sequences exhibit high SiO_2 (72-74 wt%), low-Al
302 (<14.6 wt%), low to moderate Ba, Sr, total REE (113-185 ppm) with poor to moderately
303 fractionated REE (Fig.14a in supplementary file) patterns [$(La/Yb)_N$ =4.4 -19.1] with moderate
304 Eu anomalies (Eu/Eu*=0.41 to 0.70). These characteristics together with less pronounced
305 negative Nb-Ta-Ti anomalies (Fig.14b in supplementary file) on spider diagrams and coupled
306 low Sr/Y (2.8 to 14.4), low Nb/Ta, Sr/Y, Zr/Sm, Zr/Nb, K_2O/Na_2O+CaO ratios (**see fig. 7a,**
307 **b,c**) argue for low to moderate pressure melting (10 -14 kbar) of mafic source. In-situ zircon
308 Hf isotope data [$\varepsilon Hf_{(T)}$ 2.3 to 3.1] is in conformity with trace element data indicating chondritic
309 to slightly depleted mafic source (**see fig. 8**).

310 *Eastern block: ca.3289-3276 Ma TTGs*

311 Published data[31,43] reveal younger ages of 3289 -3276 Ma for tonalitic to granodioritic
312 gneisses. Majority of the samples (except one sample) belong to low-Al (<14.3 wt%) group
313 which show high SiO_2 (70-76 wt%) have low Ba-Sr, REE (13-111 ppm) with poorly
314 fractionated (Fig. 15a in supplementary file) REE patterns [$(La/Yb)_N$=2.3-5.6] and variable Eu
315 (Eu/Eu*=0.50-1.36) and negative Nb-Ti but positive Ta and Y anomalies (Fig.15b in
316 supplementary file). These characteristics together with sub-chondritic Nb/Ta, Sr/Y, Zr/Sm,
317 K_2O/Na_2O+CaO ratios (**see fig.7a,b,c**) could be attributed to their derivation by low pressure
318 (10-12 kbar) melting of depleted to chondritic mafic source which is in agreement with their
319 incompatible element contents and in-situ zircon $\varepsilon Hf_{(T)}$ = +3.1 to +3.5[43] and whole rock $\varepsilon Nd_{(T)}$
320 = 0.3 to 1.8[31].

321 *Diapiric trondhjemites: ca.3230-3180 Ma*

Our U-Pb new zircon ages coupled with published ages indicate emplacement of trondhjemites ca. 3230-3177 Ma[31-32,43]. They exhibit high-Al (>15.0 wt%) except three samples showing low-Al (<14 wt%). Elemental characteristics like high Ba (371-724 ppm), Sr (322-735 ppm), low to moderate total REE (32-237 ppm) and moderate to highly fractionated REE [$(La/Yb)_N$=8.07-85.44, Fig.16a in supplementary file), strong negative Nb-Ti anomalies but positive or negative Sr-Y anomalies (Fig. 16b in supplementary file) indicate their origin from mafic sources at different depths. These characteristics together with high $K_2O/(Na_2O+CaO)$ but low Nb/Ta, Zr/Nb, Zr/Sm, Sr/Y, (**see figs.7a,b,c**) argue for moderate to high pressure melting (12-17 kbar) with hornblende, garnet, and ilmenite in source residue. Whole rock Nd isotope [$\varepsilon Nd_{(T)}$ = 0.4 to 1.0] and in-situ Hf ($\varepsilon Hf_{(T)}$= +2.1) data (**see fig.8**) suggest derivation of trondhjemite from short-lived mantle-derived mafic source.

Emplacement of diapiric trondhjemites and assembly of three tectonic blocks

The identification of the three distinct tectonic units in the Holenarsipur greenstone belt with independent histories is a very important discovery because their assembly into cratonic framework requires some sort of horizontal motion during Paleoarchean. In addition, the basement TTGs gneisses adjoining to Southwestern block exhibit ages ranging ca. 3430 Ma to 3300 Ma (remnants upto 3600 Ma), whilst 3430-3339 Ma adjoining to Northcentral block and 3285-3276 Ma to the western margin of the Eastern block. Strain fabrics data and U-Pb zircon ages indicate that assembly of the three tectonic units (greenstone and adjoining TTGs) coinciding with the emplacement of ca 3230-3177 Ma diapiric trondhjemites, therefore, indicating horizontal motion following terminal stage (ca. 3376 Ma) accretion of the basement. There is a consensus on the fact that majority of the Archean TTGs formed by low to medium pressure hydrous melting of young basaltic precursors with stable amphibole and/or garnet (± plagioclase, ±ilmenite) in residue[25,60]. These conditions are necessary to account for the

347 mineralogy and geochemistry of TTGs. However, the geological and tectonic process that
348 allows these conditions to be reached is still a matter of debate (e.g.,[4,8,56-57]). The ideal candidate
349 among known, and clearly identified geological processes is subduction because it can bring
350 material down into the mantle depth at rates fast enough to avoid complete dehydration of the
351 slab before reaching the hydrous solidus of wet basalt. However, rheological parameters of the
352 Eoarchean to Paleoarchean crust do not seem to be in favor of plate tectonics (e.g.,[61]).
353 Nevertheless, alternative models for plate tectonics exist and invoke horizontal motions that
354 would result in either intermittent subduction[62], formation of slices that pile downward[63], or
355 formation of duplex structures[9]. Most recent numerical modeling also propose that some
356 localized horizontal motions can develop at the margin of massive mantle plumes (e.g.,[6,58])
357 which could reconcile many of contradictory observations and fit in a fair amount of Archean
358 tectonic models involving both vertical and horizontal motions (e.g.,[4,12,48,55,59,64]). Sagduction
359 is a vertical tectonic process clearly identified in the Archean (e.g., [27,65-66]) that could possibly
360 replace the need for horizontal tectonics (e.g.,[67]). In addition, proposed sources for the
361 formation of TTGs match well with tholeiitic basalts present in greenstone belts (e.g.,[60,68]).
362 However, no clear evidence for partial melting of sinking greenstone belts has been presented
363 so far. As mentioned earlier, the western Dharwar craton presents a continuous tilted crustal
364 panel corresponding upper to lower crust which, hence, allows the sinking of high-density
365 greenstones to be followed. Yet, sinking greenstones exhibit a continuous increase in
366 metamorphic grade until granulite facies (e.g.,[42,69]) without evidence for *in-situ* partial melting.
367 This could indicate that greenstone sinking rates are too low to counterbalance dehydration
368 reaction rates and, in turn, imply that mafic lithologies would be anhydrous by the time they
369 reach their wet solidus.

370 Our model for the origin of Paleoarchean continental core in Holenarsipur region
371 involves formation of oceanic volcanic plateaus close to a microcontinent remnant prior to

372 3400 Ma (Southwestern block), followed by plume fed oceanic crust similar to modern
373 spreading centre ca. 3400 Ma (Eastern block) and its horizontal motion with eventual
374 convergence beneath micro-volcanic plateau resulted in the formation of oceanic arc **(Fig.9)**.
375 Melting of oceanic arc crust at different depths produce magmatic precursors of ca. 3350-3270
376 Ma TTGs. Assembly of oceanic arc with oceanic plateau and adjoining (>3500 Ma)
377 microcontinent in the context of shallow angle subduction with eventual slab break off ca. 3230
378 Ma caused mantle upwelling beneath arc crust/plateau led to moderate to high pressure (12-17
379 kbar) melting resulted in generation of hot trondhjemite magmas. Emplacement of these
380 trondhjemite magmas cause softening of felsic crust leading to partial convective overturn
381 driven gravitational instabilities, collapse of high density volcanics into low density felsic
382 resulting in development of dome-keel structures, culminated with metamorphism and craton
383 formation ca. 3100 Ma **(see fig.9)**. This model of diachronous evolution involving both vertical
384 addition of juvenile materials and horizontal motion is in conformity with the documented
385 accretion patterns, strain fabrics and metamorphic record (e.g.,[29]).

386
387 *Origin of cratonal core in the Western Dharwar Craton and Archean geodynamics*

388 The identification of the three genetically unrelated tectonic elements in the cratonal
389 core of WDC and their assembly is a very important discovery because this requires some sort
390 of horizontal motion to gather these distinct tectonic elements in one location. In addition, the
391 surrounding granitoid basement exhibit ages between the oldest component and that of final
392 assembly ca.3200 Ma, therefore, indicating a possible link between the gathering process and
393 the formation of the granitoids that make up the basement. Therefore, our favorite model for
394 the formation of Archean cratons is, that vertical motions in mantle upwelling zones prior to
395 3400 Ma caused melting of the base of a (stagnant) oceanic plateau lid in mantle upwelling
396 zones whilst horizontal motion initiated temporarily in the Paleoarchean ca.3350 Ma, and

perhaps the Hadean, and it was induced by boundary forces linked to the emplacement of large mantle plumes together with eruption of massive amounts of lava at the surface. Horizontal density contrasts facilitated the triggering of proto-subduction (e.g., duplex, downward piling of slices) by decoupling of tectonic elements such as oceanic crust and oceanic plateaus (e.g.,[70]). The above lines of arguments suggest that crustal fragments making up the WDC accreted through vertical motions during Eoarchean to Paleoarchean and subsequently assembled by horizontal motion of intervening (stagnant) oceanic plateau lid, eventual subduction and slab breakoff leading to generation of hot felsic magmas. Emplacement of these felsic magmas cause rheological weakening of lithosphere causing inverse density stratification, development of dome and keel structures, high T/P metamorphism resulting in craton formation.

The formation of Archean basement granitoids have been explained by oceanic crust reworking in places such as South Africa (e.g.,[10,71]) and Greenland[11,13], whereas in Pilbara [57,72] and Karelia[22] it has been argued to originate by reworking of oceanic plateau. The Western Dharwar craton presents characteristics and the differences observed among Archean cratons can certainly arise from distinct abundances of involved lithological units as well as their ages because long-term accumulation of evidence suggests that the global geodynamics evolved throughout the Archean to progressively to initiate modern-style plate tectonics[8]. There is also much debate in these localities between tectonic regimes (stagnant lid versus horizontal tectonics) but the Western Dharwar example illustrates that horizontal tectonics is necessary to assemble distinct tectonic blocks but the details regarding the origin of this horizontal motion remains uncertain. It may be, for instance, plume related (e.g.,[16]), spontaneous (e.g.,[70]), episodic[62], or scale stacking rather than actual subduction[59] but we cannot conclude on this aspect.

References

1. Sleep, NH. Edge-modulated stagnant-lid convection and volcanic passive margins. *Geochem. Geophys. Geosyst.* **8** (12), 1-15 (2007).
2. Brown, M., Johnson, T., Gardiner, NJ. Plate tectonics and the Archean Earth. *Ann. Rev. Earth Planet. Sci.* **48** (2020).
3. Moore, WB., Webb, AAG., Heat-pipe earth. *Nature* **501** (7468), 501-505 (2013).
4. Bédard, J.H., Stagnant lids and mantle overturns: implications for Archaean tectonics, magmagenesis, crustal growth, mantle evolution, and the start of plate tectonics. *Geosci. Front.* **9,** 19–49 (2018).
5. Sobolev, AV., Asafor, EV., Gurenko, AA., Arndt, NT., Batanova, VG., Portnuagin, MV., Garbe-Schonberg, D., Wilson, AH., Byerly, GR., Deep hydrous mantle reservoir provides evidence for crustal recycling before 3.3 billion years. *Nature* **571** (7766), 555-559 (2019).
6. Baes, M., Gerya, T., Sobolev, S.V., 3-D thermo-mechanical modelling of plume induced subduction initiation. *Earth Planet. Sci. Lett.* **453**, 193–203 (2016).
7. Ernst, RE., Bleeker, W., Hamilton, MA, Soderlund, U., Chamberlain, KR, Sylverster, PJ., Completing the plate tectonic revolution: a project to reconstruct pre-Pangea supercontinents using the large igneous province (LIP) record. Geological Society of America abstracts with programs 41(7), pp 368 (2009).
8. Moyen J-F, Laurent O. Archaean tectonic systems: a view from igneous rocks. *Lithos* **302-303**:99–125 (2018).
9. Komiya, T. et al., Geology of the Eoarchean, N 3.95 Ga, Nulliak supracrustal rocks in the Saglek Block, northern Labrador, Canada: The oldest geological evidence for plate tectonics, *Tectonophys*. **662**, 40-62 (2015).
10. Grosch EG, Slama J. Evidence for 3.3-billion-year-old oceanic crust in the Barberton greenstone belt, South Africa. *Geology* **45**, 695–698 (2017).
11. Bridgwater, D., McGregor, V. R. & Myers, J. S. A horizontal tectonic regime in the Archaean of Greenland and its implications for early crustal thickening. *Precam. Res*. **1**, 179-197 (1974).
12. Choukroune, P., Ludden, J.N., Chardon, D., Calvert, A.J., Bouhallier, H., Archaean crustal growth and processes: a comparision of the Superior province and the Dharwar craton India. In: Burg, J.P., Ford, M. (Eds.), Orogeny Through Time, *Geol. Soc. Spec. Publi.* **121**, 63–98 (1997).
13. Polat, A., Appel, P.W.U., Fryer, B.J., An overview of the geochemistry of Eoarchean to Mesoarchean ultramafic to mafic volcanic rocks, SW Greenland: implications for mantle depletion and petrogenetic processes at subduction zones in the early Earth. *Gond. Res.* **20 (2-3)**, 255-283 (2011).
14. Bédard, J.H., Harris, L.B., Thurston, P., The hunting of the snArc. *Precam. Res.* **229**, 20-48 (2013).
15. Calvert, A. J., Sawyer, E. W., Davis, W. J. & Ludden, J. N. Archaean subduction inferred from a mantle suture in the Superior Province. *Nature*, **375,** 670-674 (1995).
16. Gerya, T., Stern, R.J., Baes, M., Sobolev, S.V., Whattam, S.A., Plate tectonics on the Earth triggered by plume-induced subduction initiation. *Nature* **527** (7577), 221-225 (2015).
17. Rozel, A. B., Golabek, G. J., Jain, C., Tackley, P. J., & Gerya, T. Continental crust formation on early Earth controlled by intrusive magmatism. *Nature*, **545**(7654), 332–335 (2017).
18. Pearce, J.A., Geochemical fingerprinting of oceanic basalts with applications to ophiolite classification and the search for Archean oceanic crust. *Lithos* **100**, 14-48 (2008).
19. Arndt, N., The formation and evolution of the continental crust. *Geoche. Pers*. **2 (3)**, pp.405 (2013).
20. Johnson TE, Kirkland CL, Gardiner NJ, Brown M, , Smithies, R.H., Santosh, M., Secular change in TTG compositions: Implications for the evolution of Archaean geodynamics. *Earth Planet. Sci. Lett*. **505**, 65-75 (2019).
21. Smithies, R.H., et al., No evidence for high pressure melting of Earth's crust in the Archean. *Nat. Comm.* **10 (5559),** (2019).
22. Puchtel, I.S., et al., Petrology and geochemistry of crustally contaminated komatiitic basalts from the Vetreny Belt, south eastern Baltic Shield: Evidence for an early Proterozoic mantle plume beneath rifted Archean continental lithosphere. *Geochim. Cosmochim. Acta*, **61**, 1205–1222 (1997).
23. Groves, D. I., Archibald, N. J., Bettenay, L. F. & Binns, R. A. Greenstone belts as ancient marginal basins or ensialic rift zones. *Nature,* **273**, 460-461 (1978).
24. Anheeusser, C.R., Archean greenstones and associated granitic rocks - a review. *J. Af. Earth Sci.* **100,** 684-732 (2014).
25. Moyen, J.-F., Martin, H., Forty years of TTG research. *Lithos* **148,** 312-336 (2012).
26. Kaczmarek, M.A., Reddy, S.M., Nutman, A.P., Friend, C.R.L., Bennett, V.C., Earth's oldest mantle fabrics indicate Eoarchaean subduction. *Nat. comm.* **7 (10665)** (2016).

27. Bouhallier, H., Chardon, D. and Choukroune, P., Strain patterns in Archaean dome-and-basin structures: the Dharwar craton (Karnataka, South India). *Earth Plane. Sci. Lett.* **135,** 57-75 (1995).
28. Chardon, D., Jayananda, M., Chetty, T.R.K., Peucat, J-J., Precambrian continental strain and shear zone patterns: the South Indian case. *J. Geophys. Res. Solid Earth* **113**, B08402 (2008).
29. Jayananda, M., Santosh M., Aadhiseshan, K. R., Formation of Archean continental crust in the Dharwar craton, Southern India. *Earth Sci. Rev*. **181**, 12-42 (2018).
30. Radhakrishna, B.P., Naqvi, S.M., Precambrian continental crust of India and its evolution. *J. Geol.* **94**, 145–166 (1986).
31. Jayananda, M., Chardon, D., Peucat, -J.-J., Fanning, C.M., Paleo- to Mesoarchean TTG accretion and continental growth, western Dharwar craton, southern India: SHRIMP U-Pb zircon geochronology, whole-rock geochemistry and Nd-Sr isotopes. *Precam. Res.* **268**, 295–322 (2015).
32. Guitreau, M., Mukusa, S.B., Loudin, L., Krishnan, S., New constraints on early formation of western Dharwar craton (India) from igneous zircon U-Pb and Lu-Hf isotopes. *Precam. Res.* **302**: 33-49 (2017).
33. Bouhallier, H., Choukroune, P. and Ballèvre, M., Diapirism, bulk homogeneous shortening and transcurrent shearing in the Archaean Dharwar craton: the Holenarsipur area, southern India. *Precam. Res.* **63**, 43-58 (1993).
34. Nutman, AP., Chadwick, B., Ramakrishnan, M., Viswanatha, MN. SHRIMP U-Pb ages of Detrital Zircon in Sargur Supracrustal Rocks in Western Karnataka, Southern India. *J. Geol. Soc. India* **39**, 367-374 (1992).
35. Meen JK, Rogers JJ, Fullagar PD Lead isotopic composition of the Western Dharwar Craton, Southern India: evidence for distinct middle Archaean terrenes in a late Archaean Craton. *Geochim. Cosmochim. Acta* **56**, 2455–2470 (1992).
36. Jayananda, M., et al., Physical volcanology and geochemistry of Palaeoarchaean komatiite lava flows from the western Dharwar craton, southern India: implications for Archaean mantle evolution and crustal growth. *Int. Geol. Rev*. **58-13**, 1569–1595 (2016).
37. Peucat, J.-J., Bouhallier, H., Fanning, C.M., Jayananda, M., Age of Holenarsipur schist belt, relationships with the surrounding gneisses (Karnataka, south India). *J. Geol*. **103,** 701–710 (1995).
38. Naqvi, S.M., Ram Mohan, M., Rana Prathap, J.G., Srinivasa Sarma, D., Adakite–TTG connection and fate of Mesoarchaean basaltic crust of Holenarsipur nucleus, Dharwar Craton, India. *J. Asian Earth Sci*. **35**, 416–434 (2009).
39. Kunugiza, K., Kato, Y., Kano, T., Takaba, Y., Kuruma, I., Sohma, T., 1996. An Archean tectonic model of the Dharwar craton, southern India: the origin of the Holenarasipur greenstone belt (Hassan district, Karnataka) and reinterpretation of the Sargur-Dharwar relationship. *J. Asian Earth Sci.* **14 (3-4),** 149-160 (1996).
40. Swami Nath, J., Ramakrishnan, M., Early Precambrian supracrustals of Southern Karnataka. *Geol. Surv. India Mem.*, **112**, 308p (1981).
41. Naqvi SM, Allen P, Condie KC Geochemistry of some unusual early Archaean metasediments from Dharwar Craton, India. *Precam. Res* **22,** 125–147 (1983).
42. Jayananda, M., et al., Geochronological constraints on Meso-neoarchean regional metamorphism and magmatism in the Dharwar craton, southern India. *J. Asian Earth Sci.* **78**, 18–38 (2013a).
43. Ranjan, S., Upadhyay, D., Abhinay, K., Srikantappa, C., Paleoarchean and Neoarchean Tonalite-Trondhjemite-Granodiorite (TTG) and granite magmatism in the Western Dharwar Craton, southern India: implications for Archean continental growth and geodynamics. *Precam. Res*. **105630** (2020).
44. Condie, K.C., 2003. Incompatible element ratios in oceanic basalts and komatiites: Tracking deep mantle sources and continental growth rates with time. *Geochem. Geophys. Geosyst*.**4 (1)**, 1005 (2003).
45. Feng, R., Kerrich, R., Geochemical evolution of granitoids from the Archean Abitibi Southern volcanic zone and the Pontiac subprovince, Superior Province, Canada: Implications for tectonic history and source regions. *Chem. Geol.* **98 (1-2)**, 23-70 (1992).
46. Rollinson, H., Coupled evolution of Archean continental crust and subcontinental lithospheric mantle. *Geology* **38**, 1083-1086 (2010).
47. Hoffmann, J. E & MüNker, C, Polat, A. & Rosing, Minik & Schulz, Toni. The origin of decoupled Hf–Nd isotope composition in Eoarchean rocks from southern West Greenland. *Geochim. Cosmochim. Acta.* **75**. 6610-6628 (2011).
48. Martin, H., Moyen, J.-F., Guitreau, M., Blichert-Toft, J., Le Pennec, J.-L., Why Archean TTG cannot be generated by MORB melting in subduction zone. *Lithos* ***1***98-199, 1-13 (2014).
49. Barker F, Arth JG., Generation of trondhjemite-tonalite liquids and Archean bimodal trondhjemite-basalt suites. *Geology* **4** 596–600 (1976).
50. Jahn, B., Glikson, A.Y., Peucat, J.-J., Hickman, A.H., REE geochemistry and isotopic data of Archean silicic volcanics and granitoids from the Pilbara block, Western Australia: implications for early crustal evolution. *Geochim. Cosmochim. Acta* **45,** 1633-1652 (1981).

51. Moyen, J.-F., The composite Archean grey gneisses: petrological significance, and evidence for a non-unique tectonic setting for Archean crustal growth. *Lithos* **124 (1-2),** 21-36 (2011).
52. Gale, A., Dalton, C.A., Langmuir, C.H., Su, Y., Schilling, J.G., The mean composition of ocean ridge basalts. *Geochem. Geophys. Geosyst*. **14-3**, 489-518 (2013).
53. Moyen, J., Stevens, G., Experimental constraints on TTG petrogenesis: implications for Archean geodynamics. In: Been, K., Mareschal, J.-C., Condie, K.C. (Eds.), Archean Geodynamics and Environments. American Geophysical Union Monograph, Washington, DC. 149-175 (2006).
54. Adams, J., Rushmer, T., O'Neil, J., Francis, D., Hadean greenstones from Nuvvuagittuq fold belt and origin of the early continental crust. *Geology*, **40**, 363-366 (2012).
55. Guitreau, M., Blichert-Toft, J., Martin, M., Mojzsis, S.J., Albarède, F., Hafnium isotope evidence from Archean granitic rocks for deep-mantle origin of continental crust. *Earth Planet. Sci. Lett.* **337-338**, 211-223 (2012).
56. Johnson TE, Brown M, Gardiner NJ, Kirkland CL, Smithies, R.H 2017. Earth's first stable continents did not form by subduction. *Nature,* **543(7644)**: 239-242 (2017).
57. Smithies, R.H., Champion, D.C., Van Kranendonk, M.J., Formation of Paleoarchean continental crust through infracrustal melting of enriched basalt. *Earth Planet. Sci. Lett.* **281 (3-4)**, 298-306 (2009).
58. Gerya, T., Precambrian geodynamics: concepts and models. *Gond. Res.* **25,** 442–463 (2014).
59. Nagel, T.J., Hoffmann, J.E., Münker, C., Generation of Eoarchean tonalite-trondhjemite-granodiorite suite from melting thickened mafic arc crust. *Geology* **40**, 375-378 (2012).
60. Nédélec, A., Chevrel, M.O., Moyen, J.F., Ganne, J., Fabre, S., TTGs in the making: Natural evidence from Inyoni shear zone (Barberton, South Africa), *Lithos*, 153, 25-38 (2012).
61. Rey, P.F., Coltice, N., Neoarchean lithospheric strengthening and the coupling of Earth's geochemical reservoirs. *Geology* **36**, 635-638 (2008).
62. Van Hunen, J., Moyen, J.-F., Archean subduction: fact or fiction? *Ann. Rev. Earth Planet. Sci.* **40**, 195-219 (2012).
63. de Wit, M.J., On Archean granites, greenstones, cratons and tectonics: does the evidence demand a verdict? Precam. Res. **91 (1-2)**, 181-226 (1998).
64. Jayananda, M., Kano, T., Peucat, J.-J., Channabasappa, S., 3.35 Ga komatiite volcanism in the western Dharwar craton: constraints from Nd isotopes and whole rock geochemistry. *Precam. Res.***162**, 160–179 (2008).
65. Gorman, B. E., Pearce, T. H. & Birketre, T. C. On the structure of Archaean greenstone belts. *Precam. Res.*, **6**, 23-41 (1978).
66. Chardon, D., Choukroune, P., Jayananda, M., Strain patterns, de´collement and incipient sagducted greenstone terrains in the Archaean Dharwar craton (south India). *J. Struct. Geol.* **18**, 991–1004 (1996).
67. Van Kranendonk, M.J., Kröner, A., Hoffmann, J.E., Nagel, T., Anhaeusser, C.R., Just another drip: re-analysis of a proposed Mesoarchean suture from the Barberton Mountain Land, South Africa. *Precam. Res***. 254**, 19-35 (2014).
68. Rapp, R.P., Watson, E.B., Dehydration melting of metabasalt at 8–32 kbar: implications for continental growth and crust-mantle recycling. *J. Petrology* **36**, 891–931 (1995).
69. Raase, P., Raith, M., Ackermand, D., Lal, R.K., Progressive metamorphism of mafic rocks from greenschist to granulite facies in the Dharwar craton of South India. *J. Geol*. **94**, 261–282 (1986).
70. Nair, R., Chacko, T., Role of oceanic plateaus in the initiation of subduction and origin of continental crust. *Geology* **36 (7)**, 583-586 (2008).
71. Moyen, J., Stevens, G., Kisters, A., 2006. Record of mid-Archaean subduction from metamorphism in the Barberton terrain, South Africa. *Nature* **442** (7102), 559-562 (2006).
72. Van Kranendonk, M.J., Smithies, R.H., Griffin, W.L., Huston, D.L., Hickman, A.H., Champion, D.C., Anhaeusser, C.R., Pirajno, F., Making it thick: a volcanic plateau model for Paleoarchean continental lithosphere of the Pilbara and Kaapvaal cratons. In: Roberts, N.M.W., Van Kranendonk, M., Parman, S., Shirey, S., Clift, P.D. (Eds.), Continent Formation through Time. *Geol. Soc. London, Special Publications* **389**, 83-112 (2015).
73. Jenson LS., A new method of classifying alkali volcanic rocks: Ontario Division Mineral, Miscellaneous Paper, **66**:22 (1976).
74. Viljoen MJ, Viljoen FP, Pearton TN The nature and distribution of Archaean komatiite volcanics in South Africa. In: Arndt NT, Nisbet EG (eds) Komatiites. Allen and Unwin, London, 53–79 (1982).
75. Sun, S.-S., McDonough, W.F., Chemical and isotopic systematics of oceanic basalts: implications for mantle composition and processes. In: Saunders, A.D., Norry, M.J. (Eds.), Magmatism in the Ocean Basins. *Geol. Soc. London, Special publication* **42**,313-345 (1989).
76. Polat, A., Hofmann, A.W., and Rosing, M. Boninite-like volcanic rocks in the 3.7–3.8 Ga Isua greenstone belt, West Greenland: Geochemical evidence for intra-oceanic subduction zone processes in the early Earth. *Chem. Geol.* **184:** 231–254 (2002).

77. Condie, K.C., High field strength element ratios in Archean basalts: a window to evolving sources of mantle plumes: *Lithos,* **79**, 491–504 (2005).
78. Moyen, J-F., High Sr/Y and La/Yb ratios: the meaning of the "adakitic signature". *Lithos* **112 (3-4)**, 556-574 (2009).
79. Hoffmann, J.E., Zhang, C., Moyen, JF., Nagel, TJ., The formation of Tonalites-Trondhjemite-Granodiorites in Early continental crust. *Earth's Oldest Rocks*, **2nd edition**, Elsevier. 133-168 (2018).

Acknowledgements:
This work was funded by DST funded projects (ESS/16/334/2007; DST-FIST [SR/FST/ESI-146/2016(C)]) and French Agence National de la Recherche through the funded project 'Zircontinents' (ANR-17-CE31-0021) and LabEx ClerVolc (ANR-10-LABX-0006). R. V. Gireesh, Tushipokla and S.V. Balaji Manasa Rao are thanked for their assistance.

Authors contributions:

M.J and MG designed the project, generated the data. MJ wrote initial draft of the manuscript and MG contributed to writing the final version. KRA participated in the field work, sample preparation and drafting figures.

T.M and SLC have analyzed samples of greenstone volcanics for elements and Nd isotopes, and provided intellectual inputs.

Competing financial interests: The authors declare no competing financial interests

Figure captions

Fig.1. Geological sketch map showing three micro-blocks in the Holenarsipur greenstone belt and adjoining TTGs (with inset map of Peninsular India) showing greenstone units, basement granitoids and diapiric trondhjemite intrusions with age, εHf, εNd of the present study; [31-32,43].

Fig. 2. (a) Eastern block road cut section displaying section of preserved oceanic crust from pillow ultramafic through clays, BIFs, sheeted dykes, plagiogranite, gabbro/norite, layered gabbro with ultramafic and finally peridotite; (b) Interpretative E-W section of preserved oceanic crust. (c) Interpretative vertical section of the oceanic crust

Fig. 3. SW-NE interpretative cross section of crustal panel of Holenarsipur greenstone belt and adjoining basement rocks with distinct lithological assemblages corresponding to three micro-blocks.

Fig.4. (a) Al_2O_3-Fe_2O_3+TiO_2- MgO ternary plot[73] showing that volcanics of three greenstone unit are komatiite to komatiite basalt composition (b) CaO-MgO-Al_2O_3 ternary plot[74] showing dominant komatiite to komatiite basalt except two samples of Eastern block showing tholeiite composition.

Fig.5 $\varepsilon Nd_{(T)}$ versus time evolution diagram of greenstone volcanics from three blocks showing involvement of depleted mantle with minor ancient crustal contamination.

Fig.6. (a) Th/Yb versus Nb/Yb binary plot [18] indicating primitive to depleted mantle source for the southwestern, northcentral and eastern block (b) Nb/Y versus Zr/Y[77] indicating deep depleted to primitive mantle reservoir source for the samples from southwestern, northcentral and eastern block greenstone volcanics. (c) Zr/Nb versus Nb/Th plot[77] indicating oceanic plateau for SW block, arc to oceanic plateau for North central block and N-MORB to oceanic plateau for Eastern block. Arrows indicate effects of batch melting (F) and subduction (SUB); PM, primitive mantle; DM, shallow depleted mantle; ARC, arc related basalts; NMORB, normal ocean ridge basalt; OIB, oceanic island basalt; DEP, deep depleted mantle; EN, enriched component.

Fig. 7. (a) Nb/Ta vs Zr/Sm plot [47] explaining the origin of TTG melt from different source composition, (b) Nb/Ta vs Sr/Y plot[78]; (c) K_2O/(Na_2O+CaO) vs Sr/Y plot[79] representing the different pressure level at which the studied

samples generated from the mantle. Lines correspond to melting models derived from experimental database, as in [51,78], at different pressures and for two sources, an MORB and a more enriched mafic rock.

Fig.8. ε_{Hf} versus age diagram for zircons from granitoids exposed within Southwestern, Northcentral and Eastern blocks around the Holenarsipur Belt (Western Dharwar craton). Also shown are the evolution of the depleted mantle, assuming a present day ε_{Hf} of +17, of an arc mantle (present day ε_{Hf} of +13), of a typical basalt, TTG and zircon formed from an arc mantle at 3700 Ma. Values indicated next to the evolution lines of basalt, TTG and zircon correspond to average $^{176}Lu/^{177}Hf$. CHUR refers to Chondritic Uniform Reservoir.

Fig.9. Proposed tectonic model for origin of Paleoarchean cratons: (a) Formation of plume fed volcanic plateau on stagnant lid ca. >3500 Ma close to remnant of micro-continent; (b) Continued plume impact caused low pressure melting of stagnant lid to produce magmatic precursors of 3500-3400 Ma TTGs; (c) Initiation of oceanic spreading centre in the east during 3400-3350 Ma caused horizontal motion of stagnant lid with eventual subduction beneath volcanic plateau resulted in the development oceanic island arc system; (d) Continued subduction with accumulation hot magmas (generated at greater depth) at the base of arc crust cause melting of arc crust at different depth producing TTG magmas during ca. 3350-3270 Ma; (e) Continued subduction with assembly of oceanic crust, island arc and volcanic plateau and eventual slab breakoff lead to the asthenosphere upwelling caused melting of lower crust/upper most mantle generated hot trondhjemite magmas during ca.3200 Ma; emplacement hot trondhjemite magmas into crust caused partial convective overturn soften crust leading formation of dome and keel structure followed by metamorphism and cratonization ca. 3200-3150 Ma.

Fig. 1

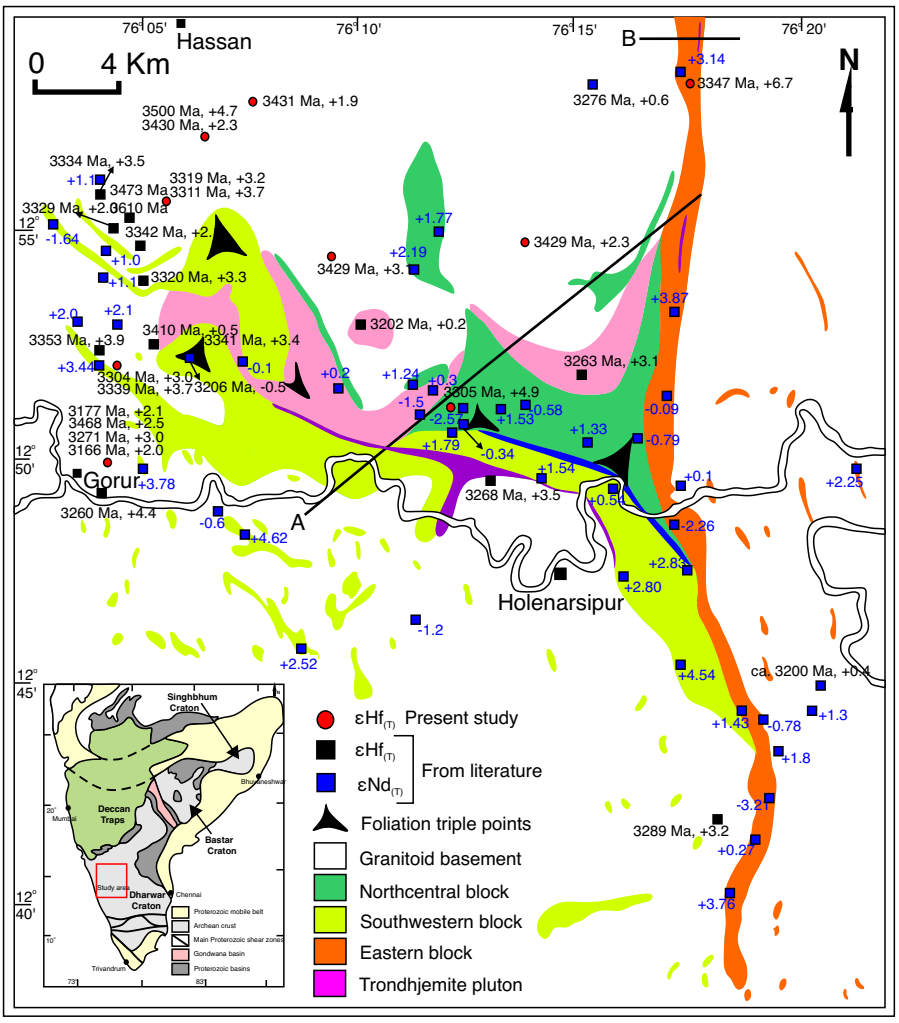
Hassan
Gorur
Holenarsipur
A
B
N
0 4 Km
3500 Ma, +4.7
3430 Ma, +2.3
3431 Ma, +1.9
3276 Ma, +0.6
3347 Ma, +6.7
3334 Ma, +3.5
3319 Ma, +3.2
3473 Ma
3311 Ma, +3.7
3342 Ma, +2.
3320 Ma, +3.3
3429 Ma, +2.3
3429 Ma, +3.1
3202 Ma, +0.2
3410 Ma, +0.5
3353 Ma, +3.9
3341 Ma, +3.4
3304 Ma, +3.0
3339 Ma, +3.7
3206 Ma, -0.5
3263 Ma, +3.1
3305 Ma, +4.9
3177 Ma, +2.1
3468 Ma, +2.5
3271 Ma, +3.0
3166 Ma, +2.0
3268 Ma, +3.5
3260 Ma, +4.4
3289 Ma, +3.2
ca. 3200 Ma, +0.4
Singhbhum Craton
Deccan Traps
Bastar Craton
Dharwar Craton
Study area
Mumbai
Chennai
Trivandrum
Proterozoic mobile belt
Archean crust
Main Proterozoic shear zones
Gondwana basin
Proterozoic basins
εHf(T) Present study
εHf(T)
εNd(T)
From literature
Foliation triple points
Granitoid basement
Northcentral block
Southwestern block
Eastern block
Trondhjemite pluton

Fig. 2

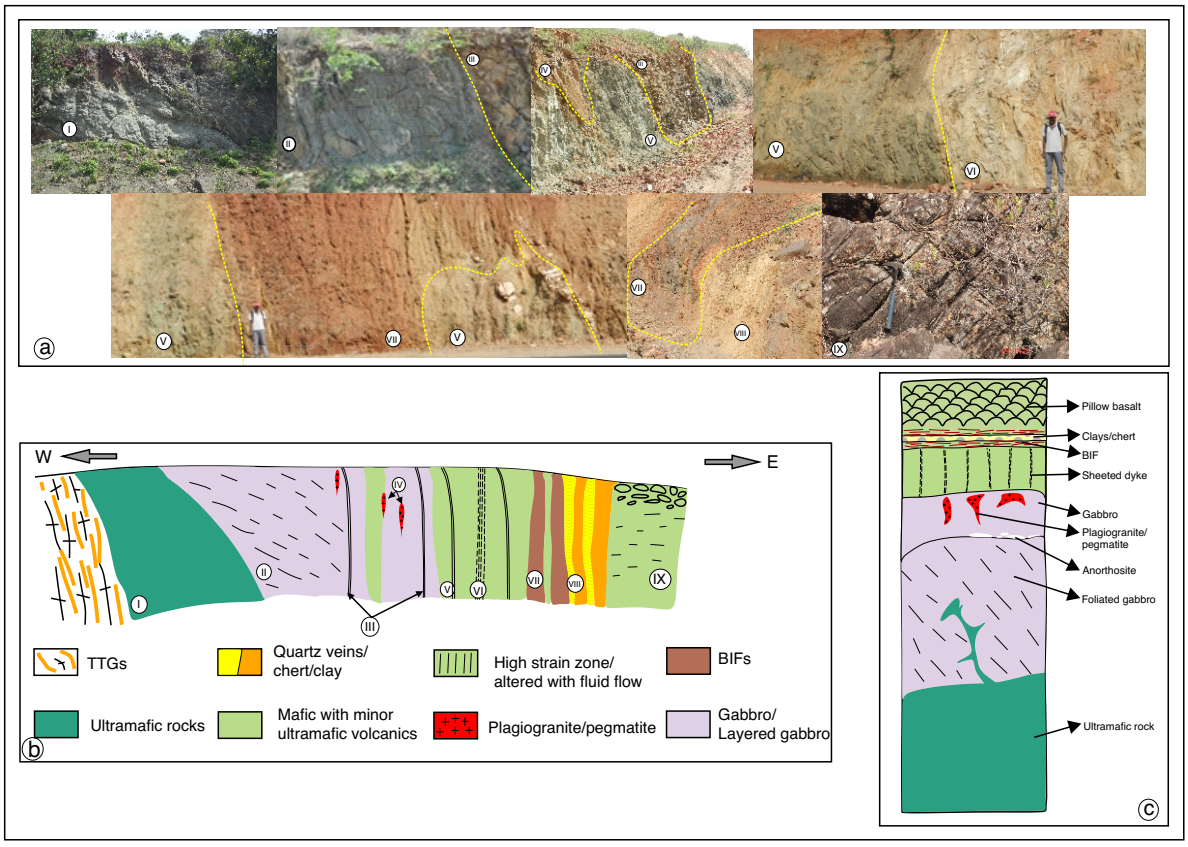
a
W
E
b
TTGs
Quartz veins/ chert/clay
High strain zone/ altered with fluid flow
BIFs
Ultramafic rocks
Mafic with minor ultramafic volcanics
Plagiogranite/pegmatite
Gabbro/ Layered gabbro
Pillow basalt
Clays/chert
BIF
Sheeted dyke
Gabbro
Plagiogranite/ pegmatite
Anorthosite
Foliated gabbro
Ultramafic rock
c

Fig. 3

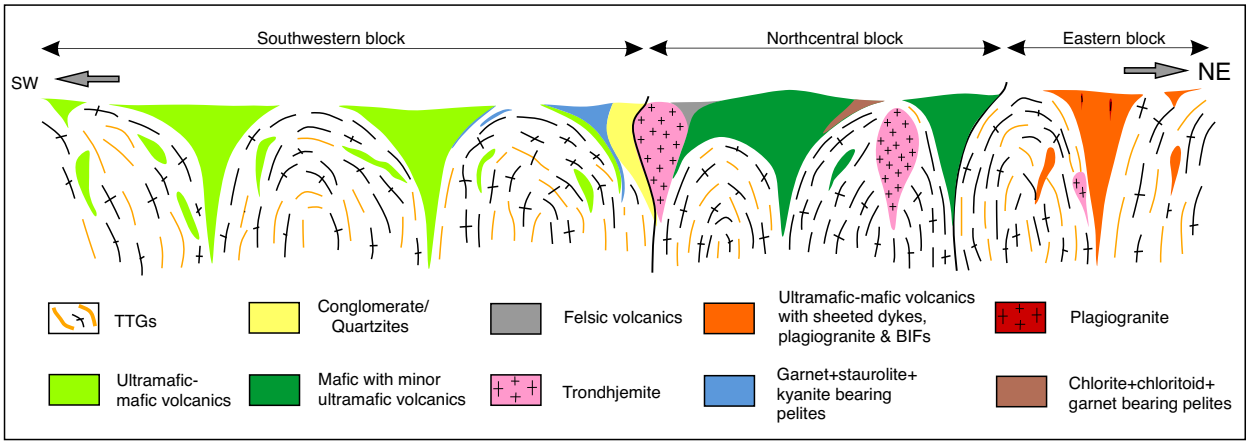

Fig. 4a,b

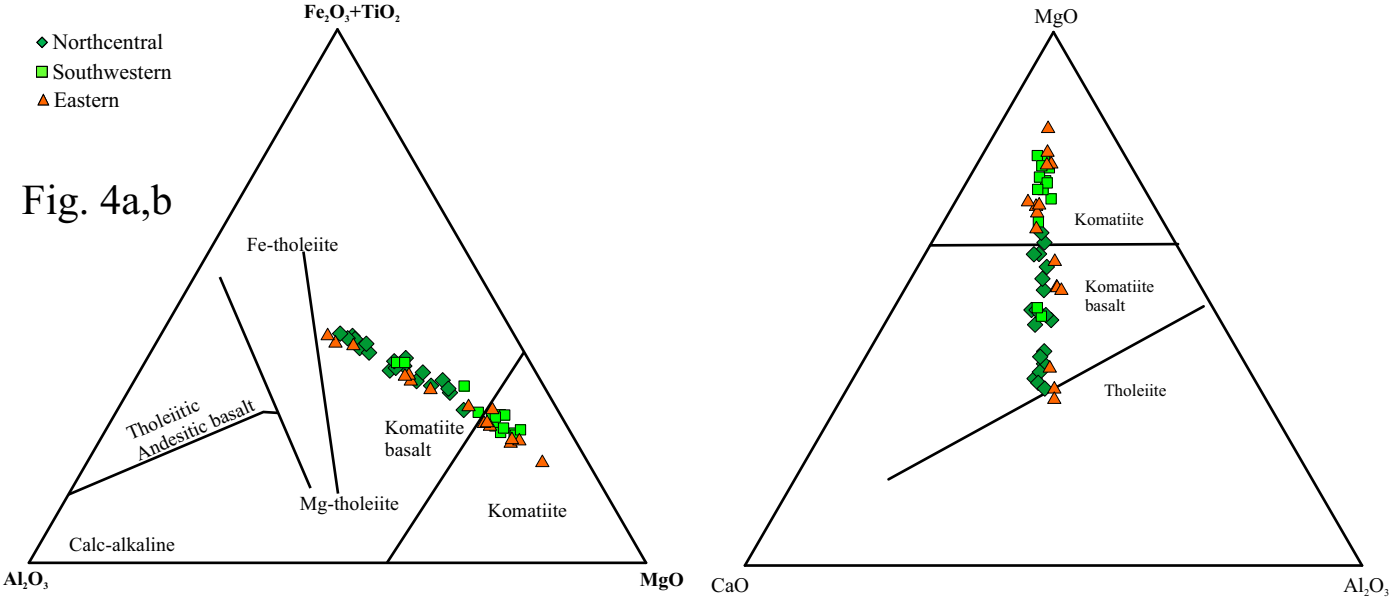

Fig. 5

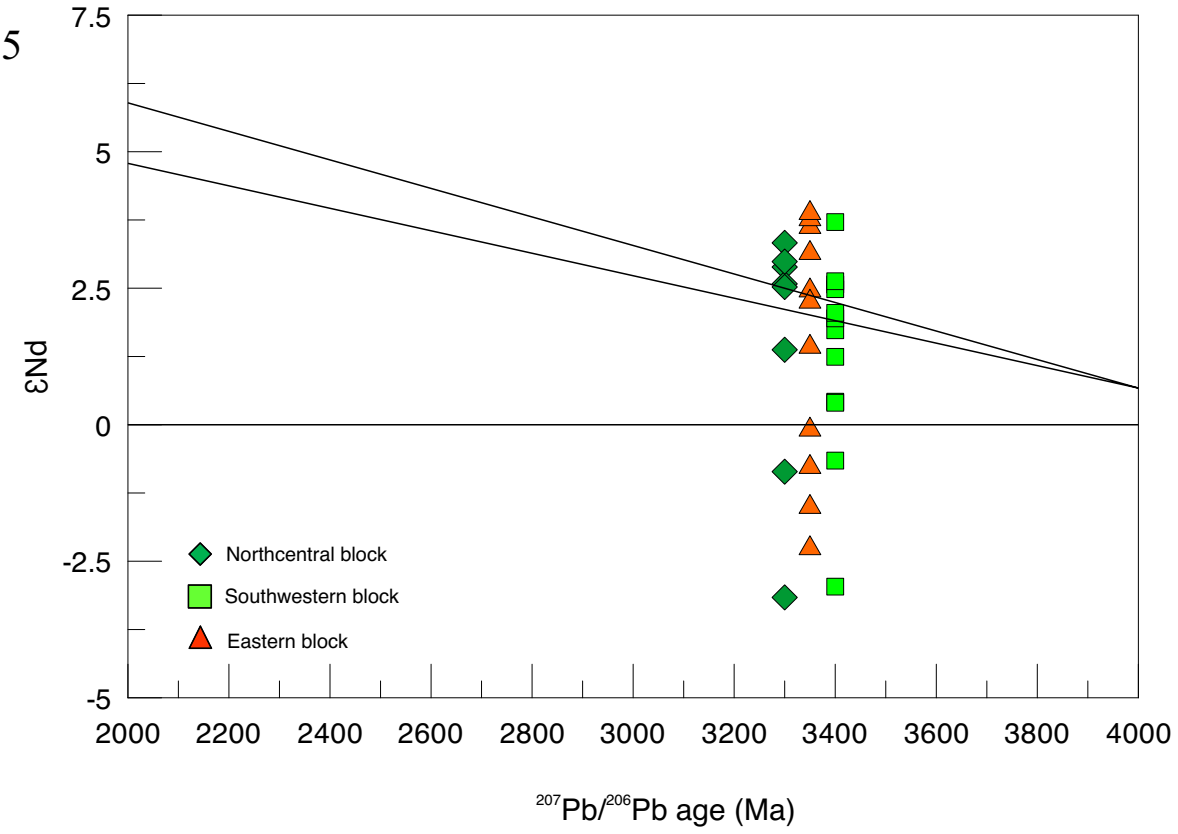

Fig. 6a

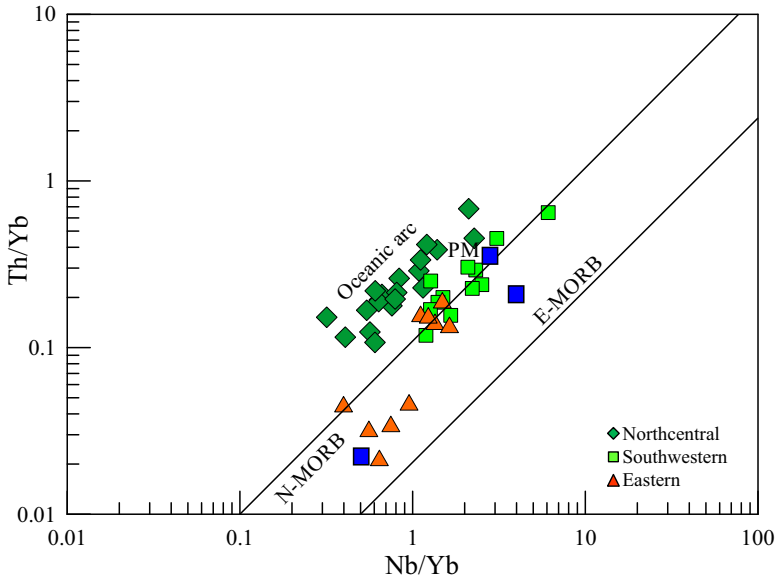

Fig. 6b

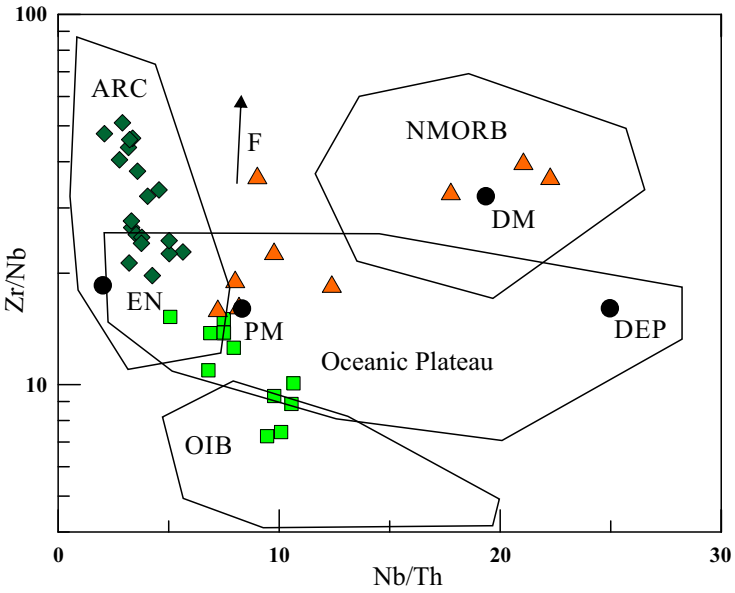

Fig. 6c

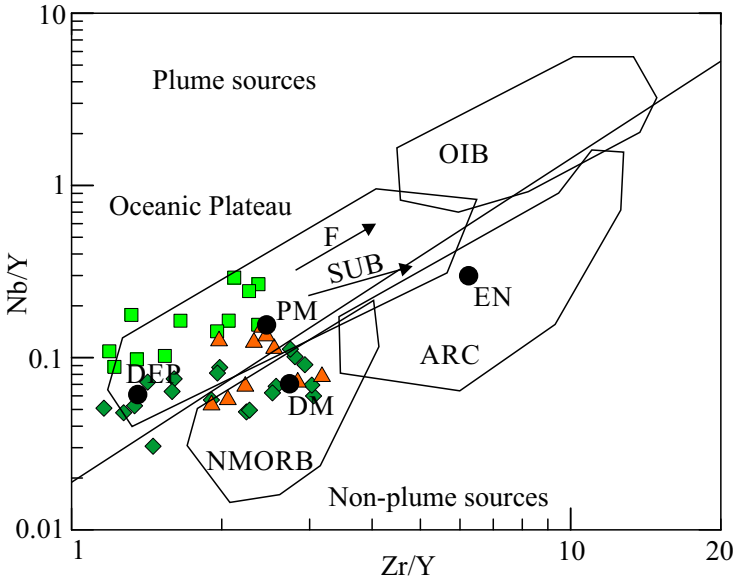

Fig. 7a

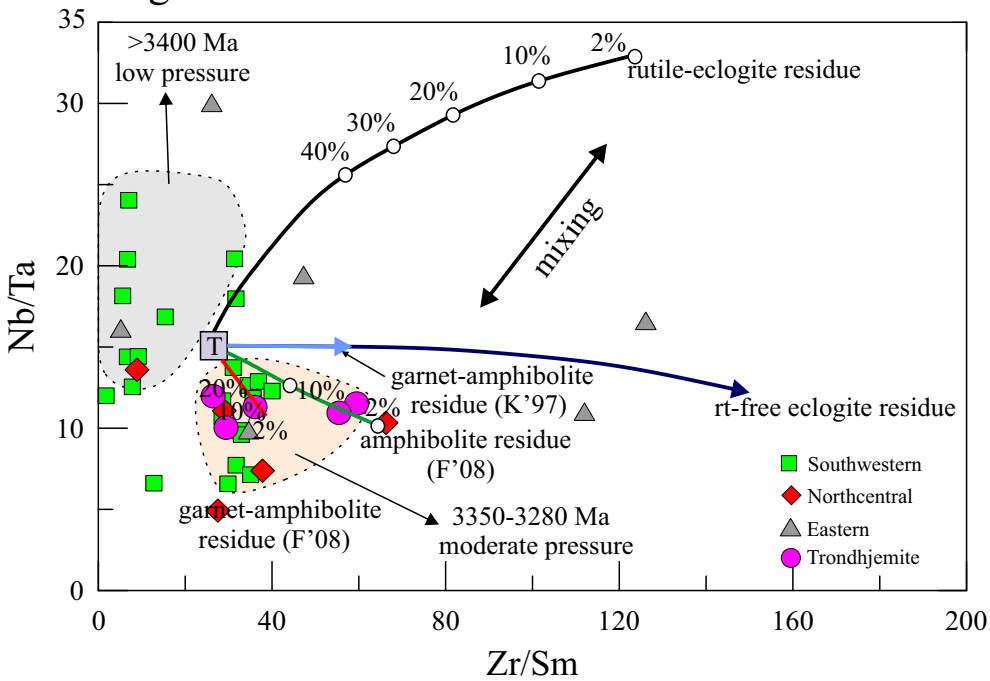

Fig. 7b

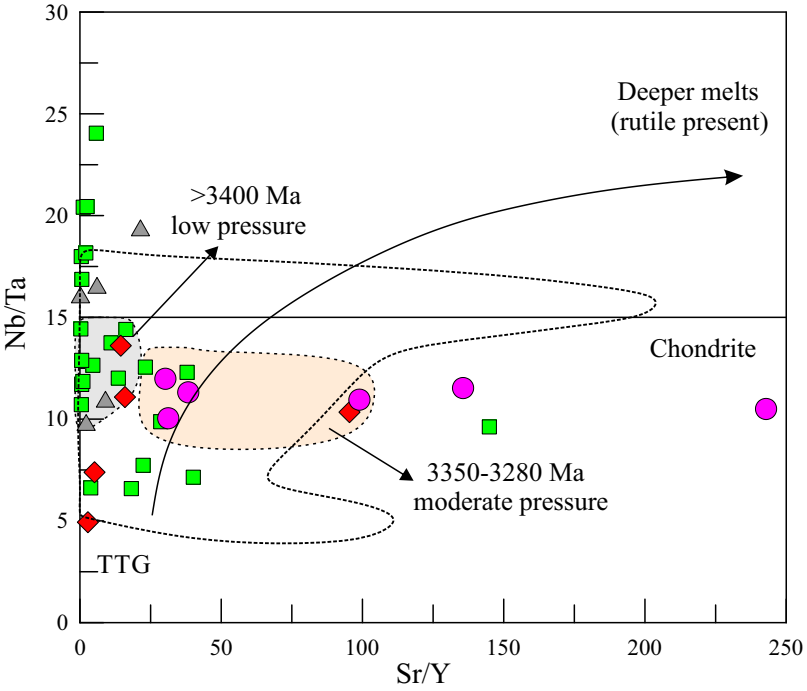

Fig. 7c

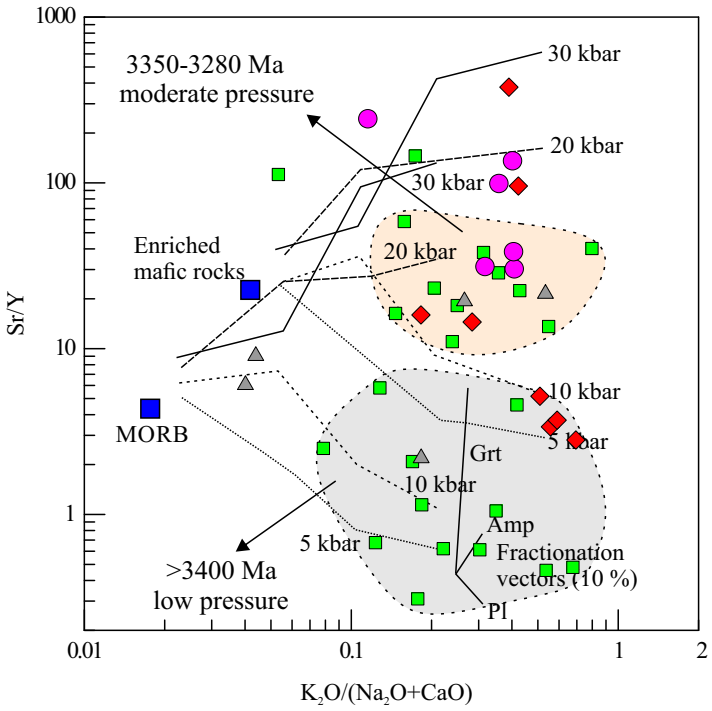

Fig. 8

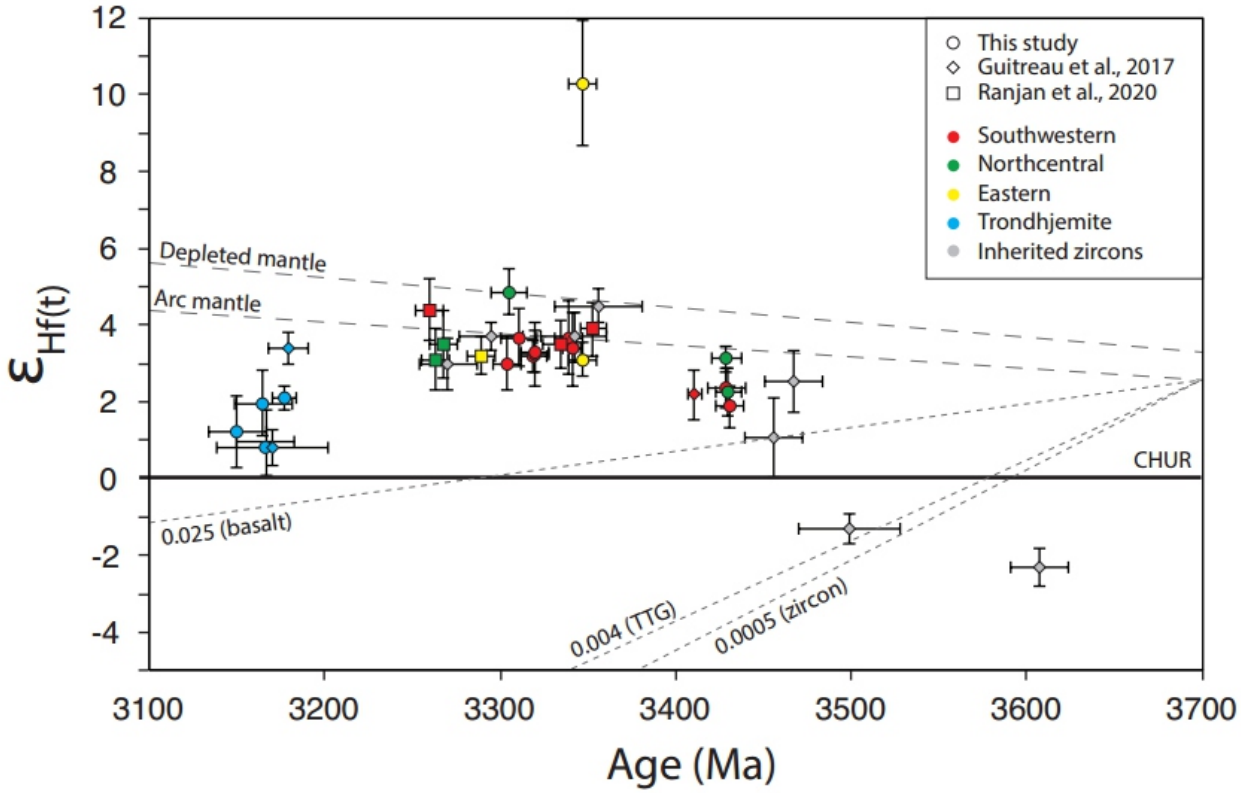

Fig. 9

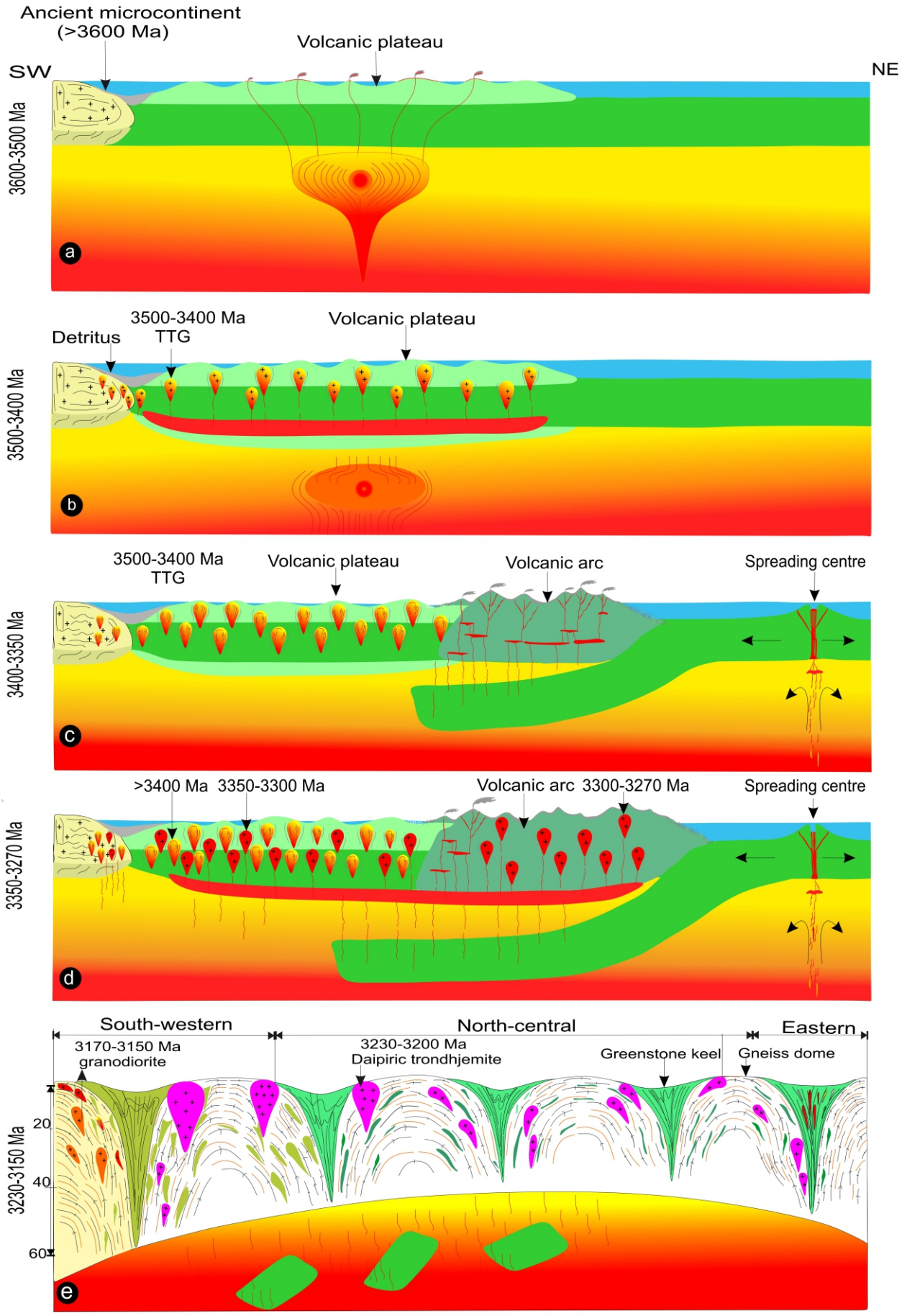
Ancient microcontinent
(>3600 Ma)
Volcanic plateau
SW
NE
3600-3500 Ma
a
3500-3400 Ma
TTG
Detritus
Volcanic plateau
3500-3400 Ma
b
3500-3400 Ma
TTG
Volcanic plateau
Volcanic arc
Spreading centre
3400-3350 Ma
c
>3400 Ma
3350-3300 Ma
Volcanic arc
3300-3270 Ma
Spreading centre
3350-3270 Ma
d
South-western
North-central
Eastern
3170-3150 Ma
granodiorite
3230-3200 Ma
Daipiric trondhjemite
Greenstone keel
Gneiss dome
3230-3150 Ma
20
40
60
e

Figures

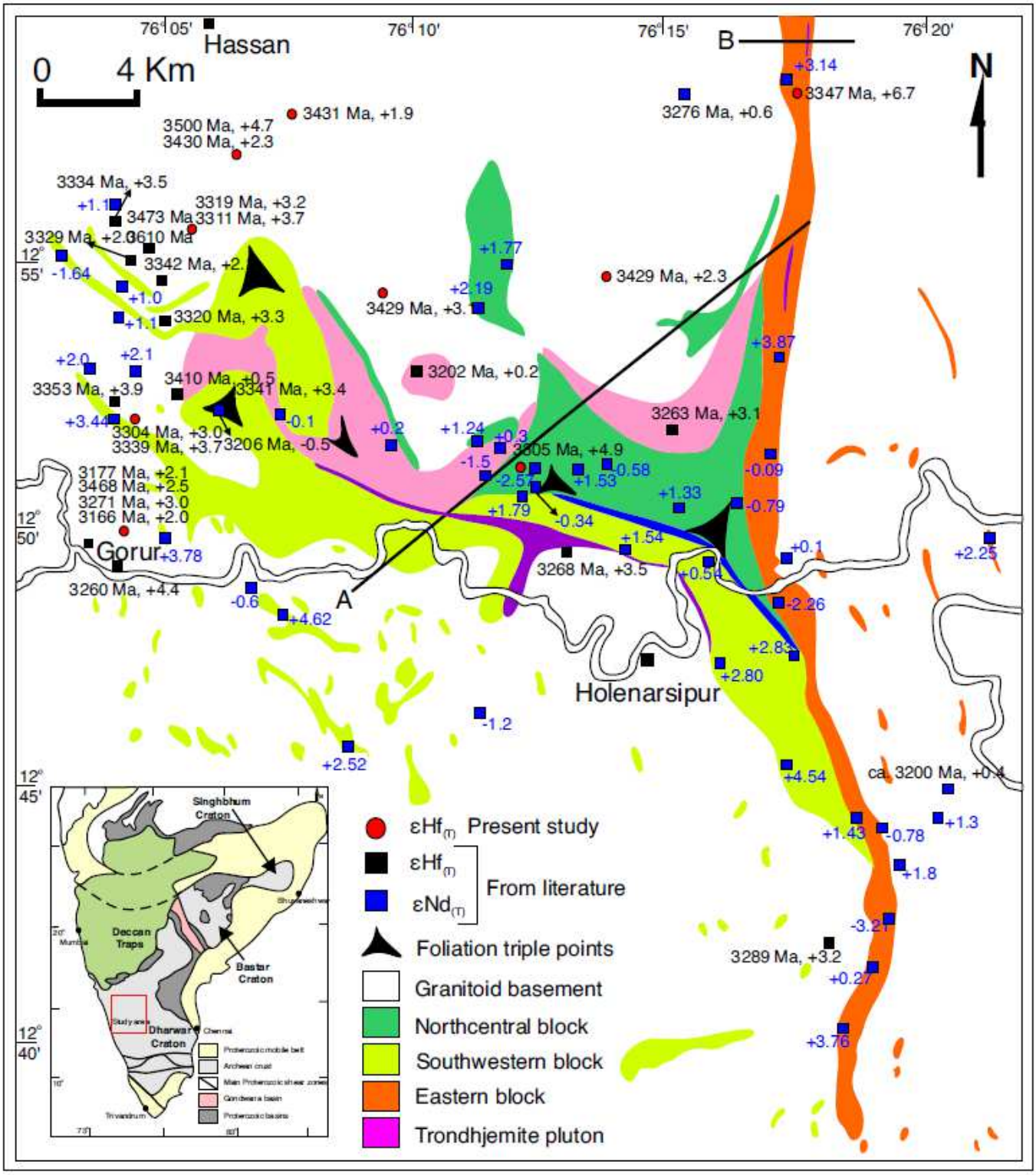

Figure 1

Geological sketch map showing three micro-blocks in the Holenarsipur greenstone belt and adjoining TTGs (with inset map of Peninsular India) showing greenstone units, basement granitoids and diapiric trondhjemite intrusions with age, εHf, εNd of the present study; 31-32,43.

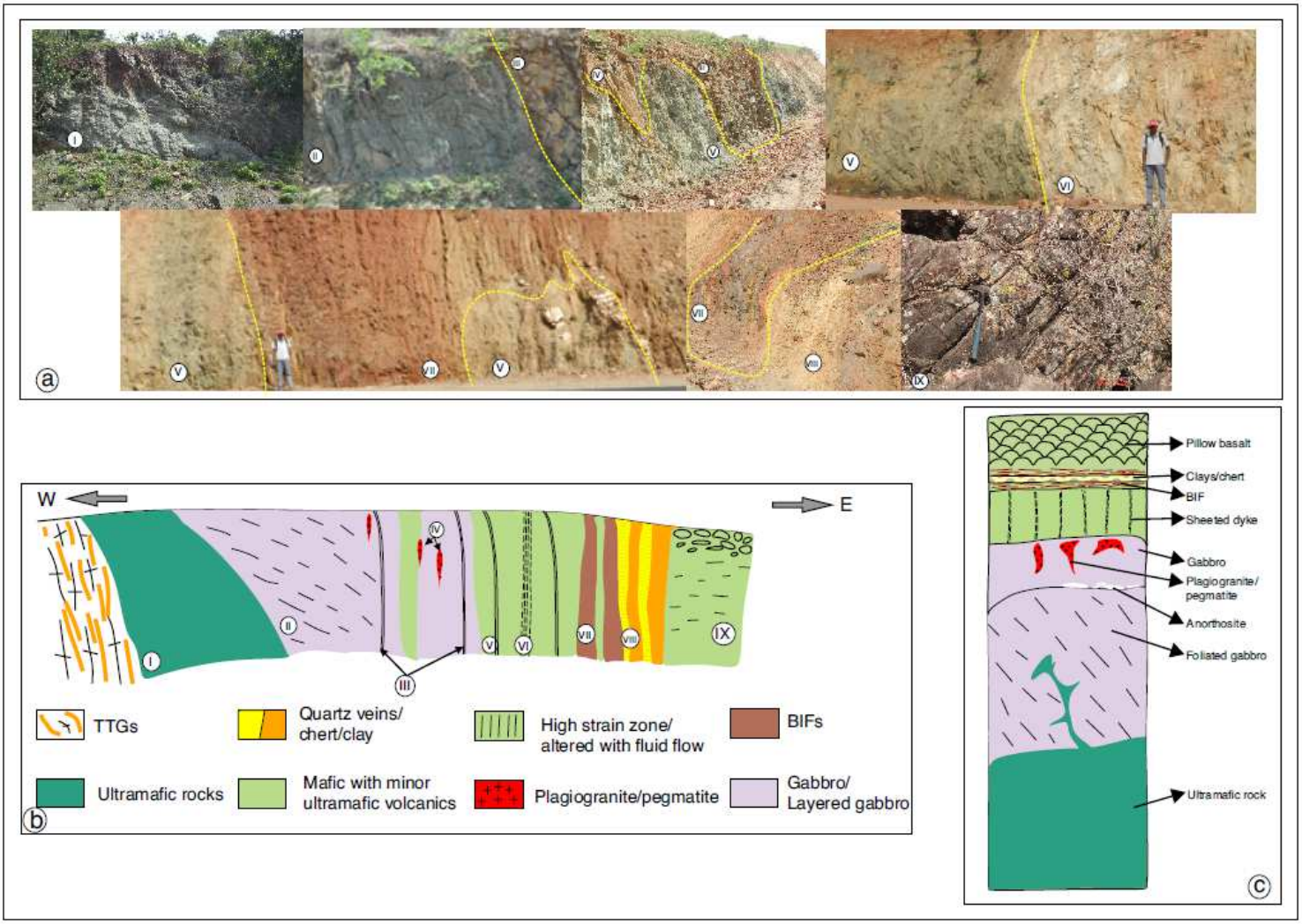

Figure 2

(a) Eastern block road cut section displaying section of preserved oceanic crust from pillow ultramafic through clays, BIFs, sheeted dykes, plagiogranite, gabbro/norite, layered gabbro with ultramafic and finally peridotite; (b) Interpretative E-W section of preserved oceanic crust. (c) Interpretative vertical section of the oceanic crust

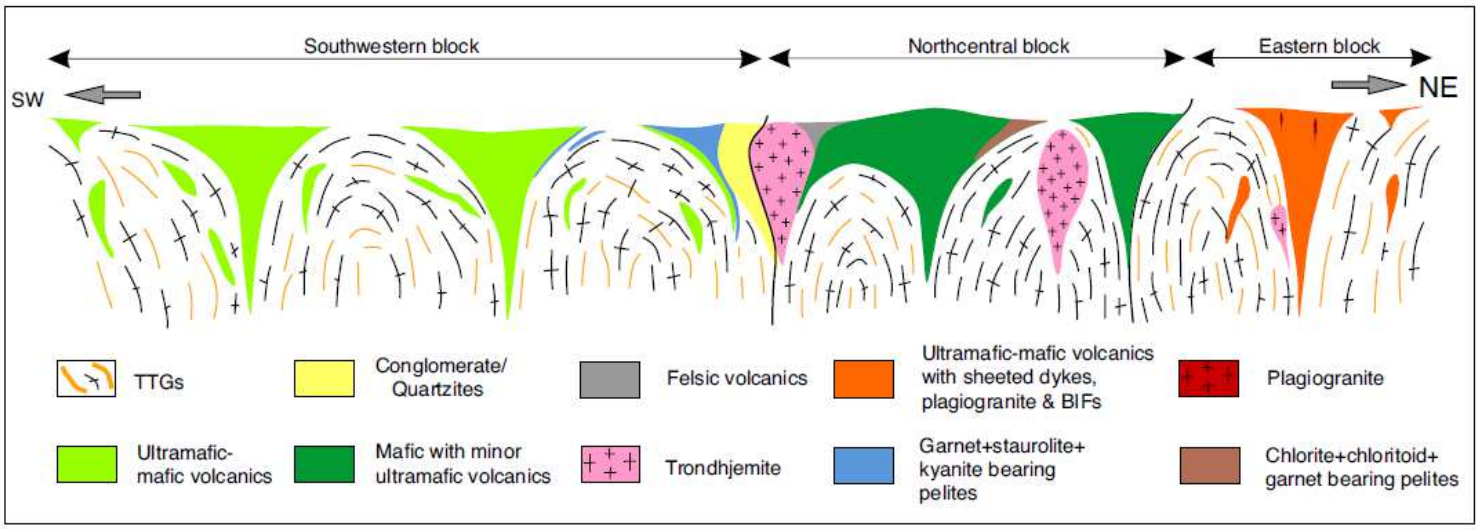

Figure 3

SW-NE interpretative cross section of crustal panel of Holenarsipur greenstone belt and adjoining basement rocks with distinct lithological assemblages corresponding to three micro-blocks.

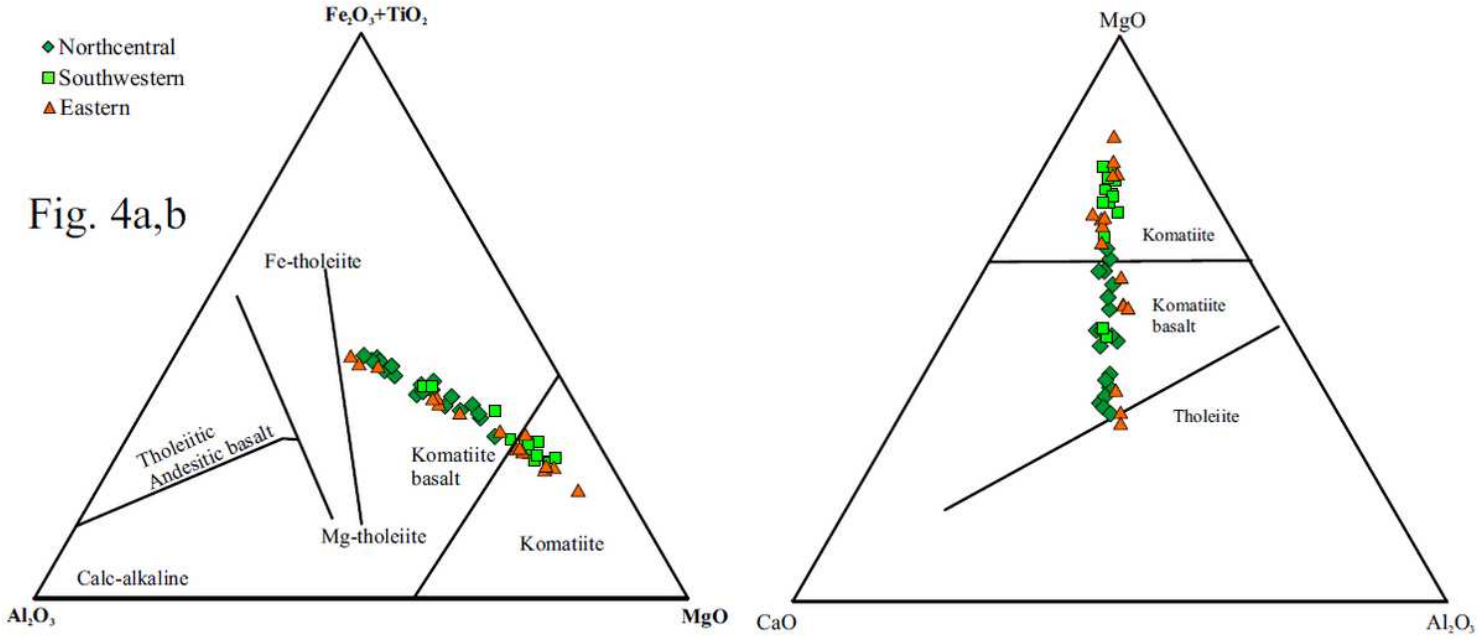

Figure 4

(a) Al2O3-Fe2O3+TiO2- MgO ternary plot73 showing that volcanics of three greenstone unit are komatiite to komatiite basalt composition (b) CaO-MgO-Al2O3 ternary plot74 showing dominant komatiite to komatiite basalt except two samples of Eastern block showing tholeiite composition.

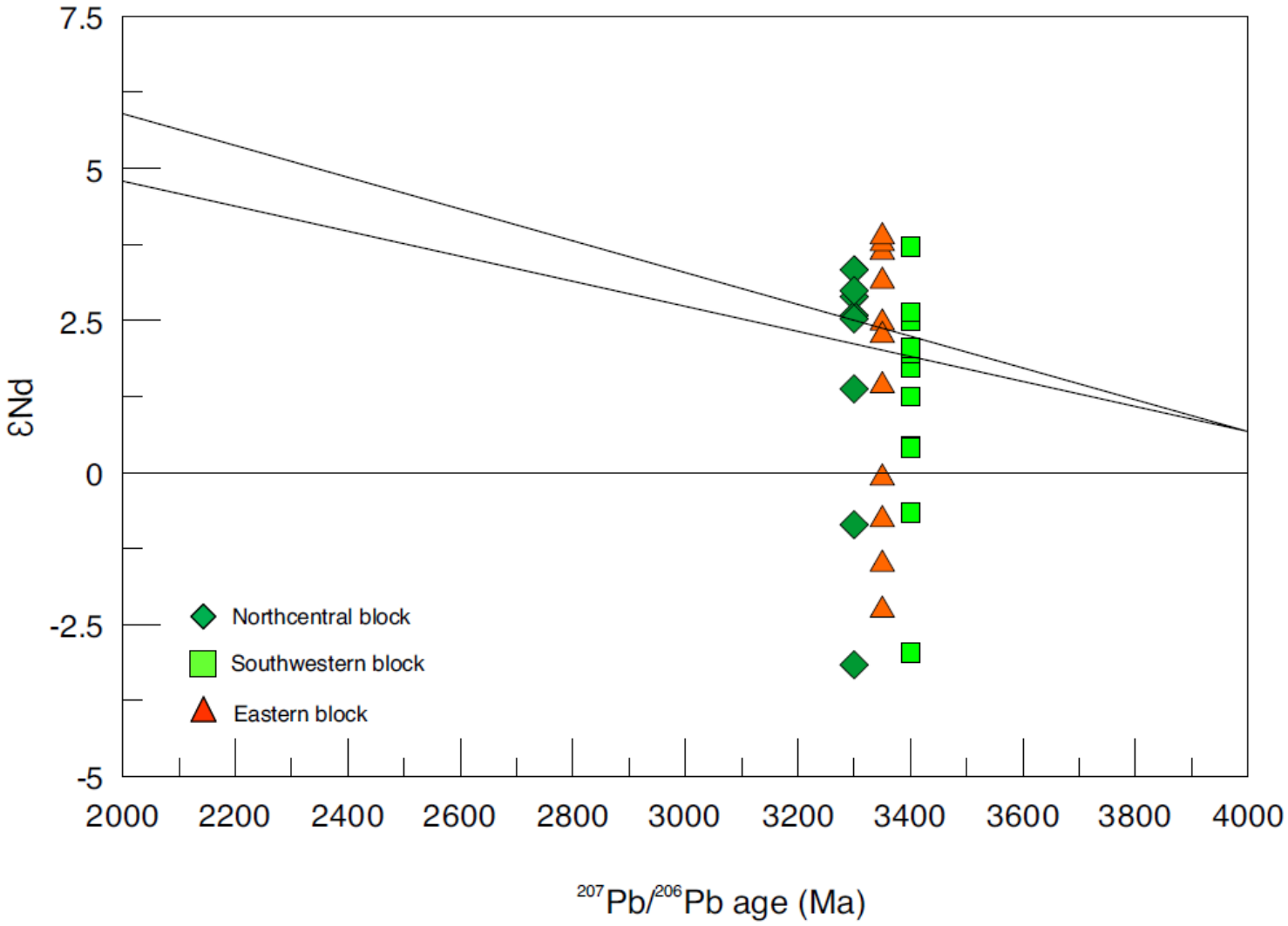

Figure 5

Nd(T) versus time evolution diagram of greenstone volcanics from three blocks showing involvement of depleted mantle with minor ancient crustal contamination.

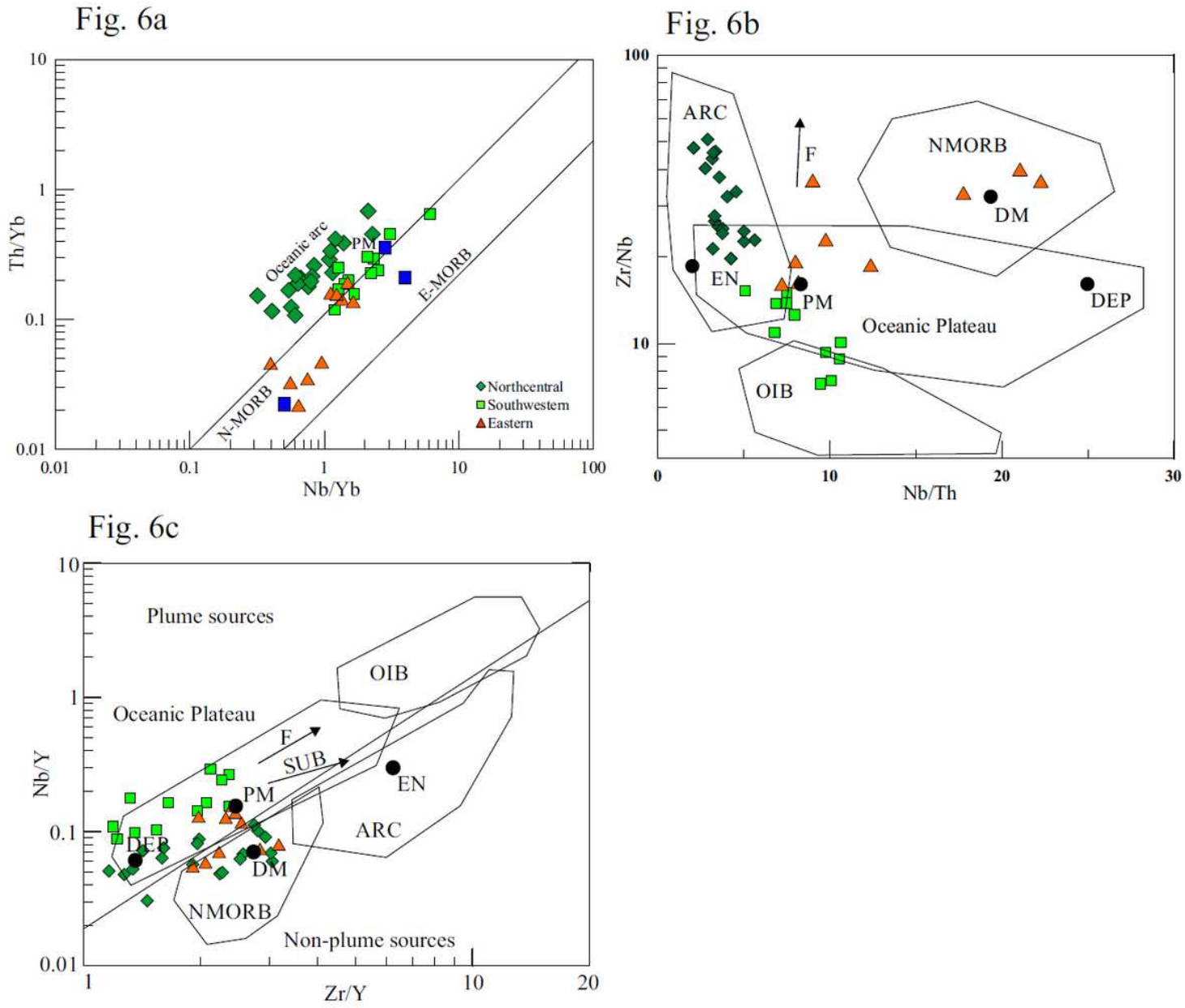

Figure 6

(a) Th/Yb versus Nb/Yb binary plot 18 indicating primitive to depleted mantle source for the southwestern, northcentral and eastern block (b) Nb/Y versus Zr/Y77 indicating deep depleted to primitive mantle reservoir source for the samples from southwestern, northcentral and eastern block greenstone volcanics. (c) Zr/Nb versus Nb/Th plot77 indicating oceanic plateau for SW block, arc to oceanic plateau for North central block and N-MORB to oceanic plateau for Eastern block. Arrows indicate effects of batch melting (F) and subduction (SUB); PM, primitive mantle; DM, shallow depleted mantle; ARC, arc related basalts; NMORB, normal ocean ridge basalt; OIB, oceanic island basalt; DEP, deep depleted mantle; EN, enriched component.

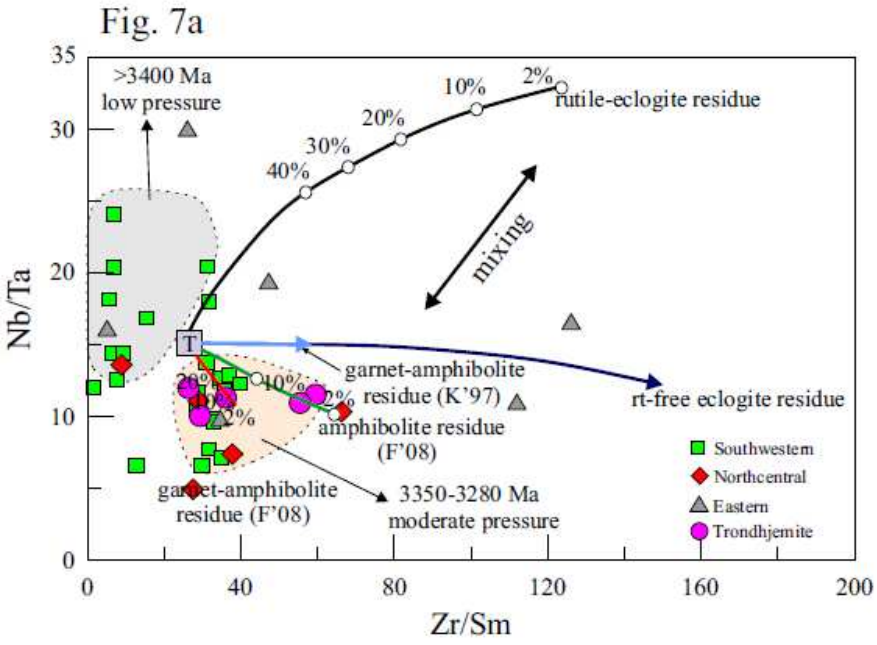

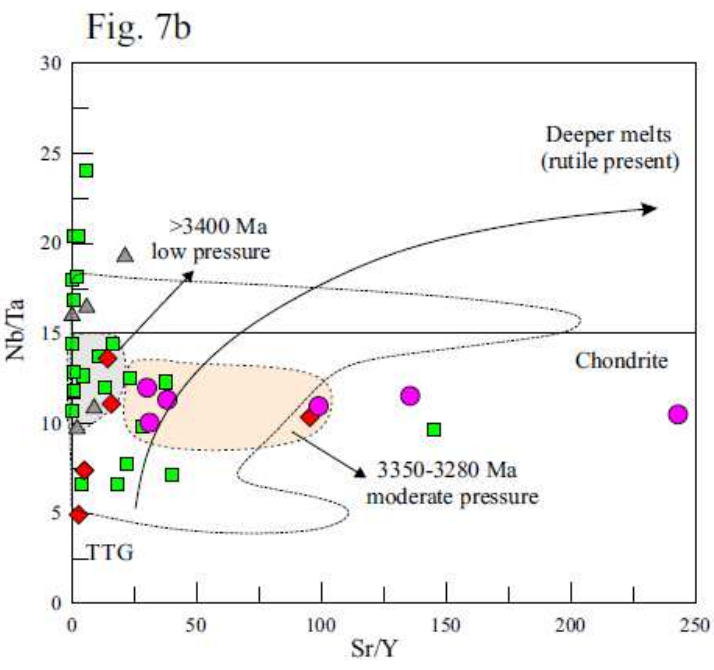

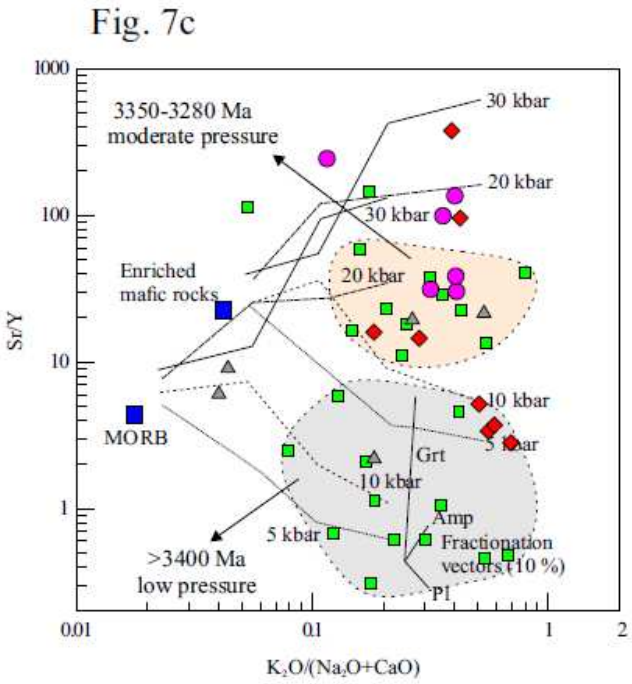

Figure 7

(a) Nb/Ta vs Zr/Sm plot 47 explaining the origin of TTG melt from different source composition, (b) Nb/Ta vs Sr/Y plot78; (c) K2O/(Na2O+CaO) vs Sr/Y plot79 representing the different pressure level at which the studied samples generated from the mantle. Lines correspond to melting models derived from experimental database, as in 51,78, at different pressures and for two sources, an MORB and a more enriched mafic rock.

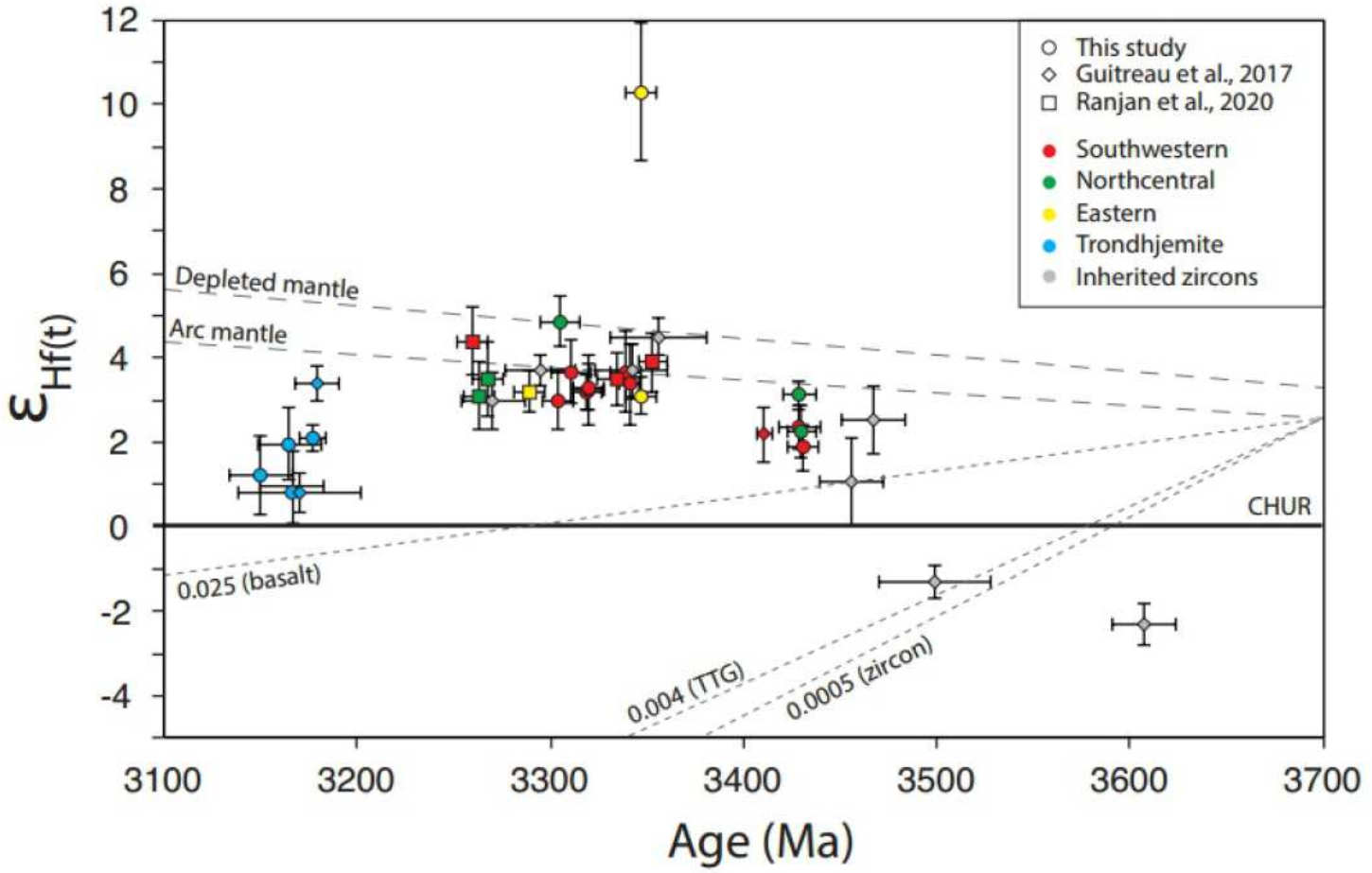

Figure 8

Hf versus age diagram for zircons from granitoids exposed within Southwestern, Northcentral and Eastern blocks around the Holenarsipur Belt (Western Dharwar craton). Also shown are the evolution of the depleted mantle, assuming a present day Hf of +17, of an arc mantle (present day Hf of +13), of a typical basalt, TTG and zircon formed from an arc mantle at 3700 Ma. Values indicated next to the evolution lines of basalt, TTG and zircon correspond to average 176Lu/177Hf. CHUR refers to Chondritic Uniform Reservoir.

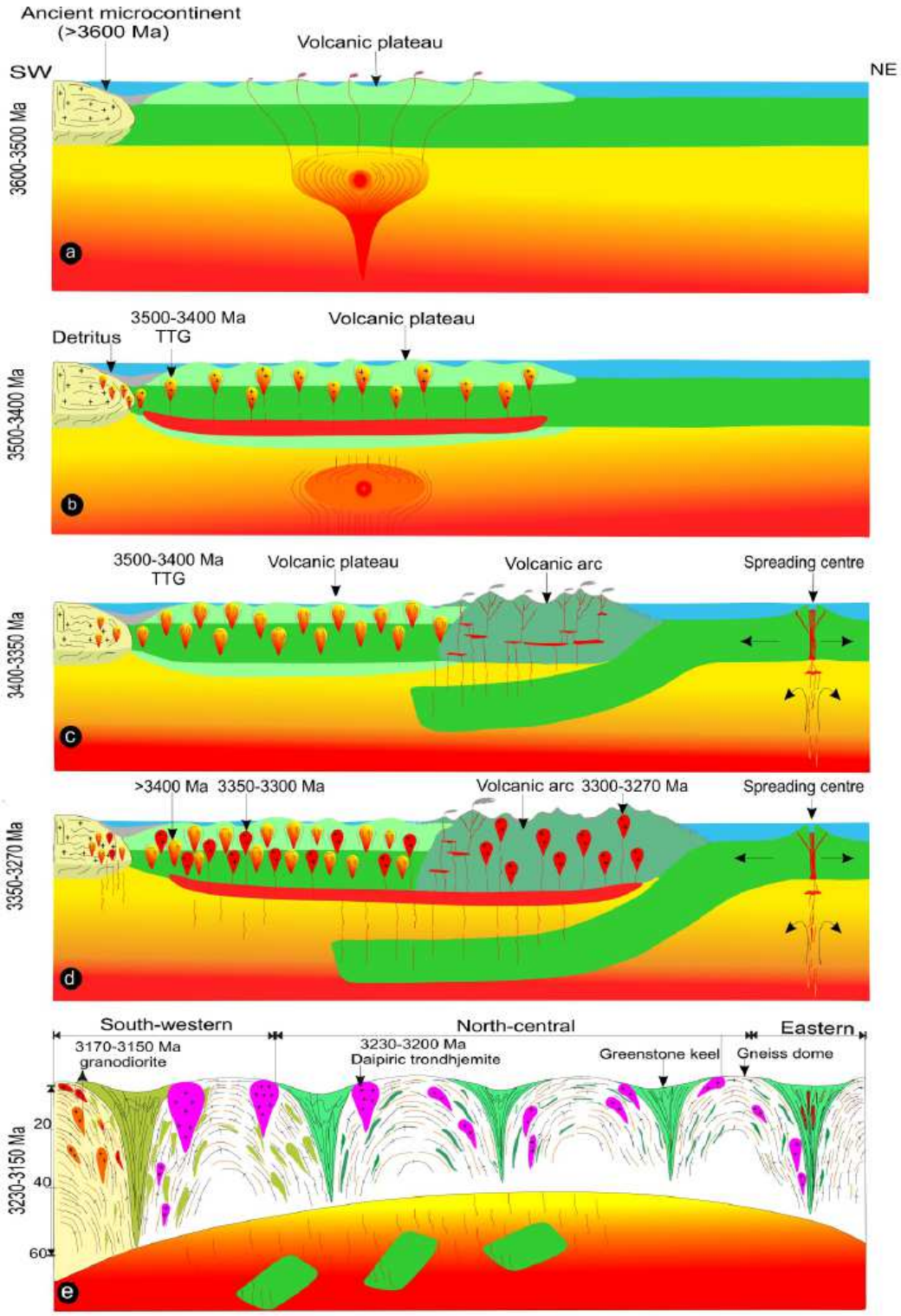

Figure 9

Proposed tectonic model for origin of Paleoarchean cratons: (a) Formation of plume fed volcanic plateau on stagnant lid ca. >3500 Ma close to remnant of micro-continent; (b) Continued plume impact caused low pressure melting of stagnant lid to produce magmatic precursors of 3500-3400 Ma TTGs; (c) Initiation of oceanic spreading centre in the east during 3400-3350 Ma caused horizontal motion of stagnant lid with eventual subduction beneath volcanic plateau resulted in the development oceanic

island arc system; (d) Continued subduction with accumulation hot magmas (generated at greater depth) at the base of arc crust cause melting of arc crust at different depth producing TTG magmas during ca. 3350-3270 Ma; (e) Continued subduction with assembly of oceanic crust, island arc and volcanic plateau and eventual slab breakoff lead to the asthenosphere upwelling caused melting of lower crust/upper most mantle generated hot trondhjemite magmas during ca.3200 Ma; emplacement hot trondhjemite magmas into crust caused partial convective overturn soften crust leading formation of dome and keel structure followed by metamorphism and cratonization ca. 3200-3150 Ma.

Supplementary Files

This is a list of supplementary files associated with this preprint. Click to download.

- Jayanandaetal2020Naturecommunicationssupplementarymanuscript.pdf